Unravelling the Anticancer Potential of a Square Planar Copper Complex: Toward Non-platinum Chemotherapy

Manzoor Ahmad Malik
Jamia Millia Islamia
Md Kausar Raza
Indian Institute of Science Bangalore
Arif Mohammed
Jeddah University
Mohmmad Younus Wani (mwani@uj.edu.sa)
Jeddah University
Athar Adil Hashmi
Jamia Millia Islamia

Research Article

Keywords: Coordination compounds, platinumbased complexes, platinum based chemotherapy

Posted Date: February 22nd, 2021

DOI: https://doi.org/10.21203/rs.3.rs-208823/v1

Version of Record: A version of this preprint was published at RSC Advances on January 1st, 2021. See the published version at https://doi.org/10.1039/D1RA06227A.

Unravelling the anticancer potential of a square planar copper complex: toward non-platinum chemotherapy

Manzoor Ahmad Malik[1], Md Kausar Raza[2], Arif Mohammed[3], Mohmmad Younus Wani[4*], Athar Adil Hashmi[1*]

[1]Bioinorganic Lab., Department of Chemistry, Jamia Millia Islamia, New Delhi 110025, India.[2]Department of Inorganic and Physical Chemistry, Indian Institute of Science, Bangalore 560012, India.[3]University of Jeddah, College of Science, Department of Biology, Jeddah 21589, Saudi Arabia.[4]University of Jeddah, College of Science, Department of Chemistry, Jeddah 21589, Saudi Arabia.

Correspondence: mwani@uj.edu.sa (MYW); ahashmi@jmi.ac.in (AAH)

Abstract

Coordination compounds from simple transition metals are robust substitutes for platinum-based complexes due to their remarkable anticancer properties. In a quest to find new metal complexes that could substitute or augment the platinum based chemotherapy we synthesized three transition metal complexes **C1-C3** with Cu(II), Ni(II), and Co(II) as the central metal ions, respectively, and evaluated them for their anticancer activity against human keratinocyte (HaCaT) cell line and human cervical cancer (HeLa) cell lines. These complexes showed different activity profiles with the square planar copper complex **C1** being the most active with IC_{50} values lower than the widely used anticancer drug-cisplatin. Assessment of the morphological changes by DAPI staining and ROS generation by DCFH-DA assay exposed that the cell death occurred by caspase-3 mediated apoptosis. **C1** displayed interesting interactions with Ct-DNA, evidenced by absorption spectroscopy and validated by docking studies. Together, our results suggest that binding of the ligand to the DNA-binding domain of p53 tumor suppressor (p53DBD) protein and the induction of apoptotic hallmark protein, caspase-3 upon treatment with the metal complex could be positively attributed to a higher level of ROS and the subsequent DNA damage (oxidation), generated by compound **C1**, that could well explain the interesting anticancer activity observed for this complex.

1. Introduction

Cancer, also called malignancy, is one of the major health problems in the world and has a major impact on the socioeconomic condition of several countries. It is one of the prominent causes of death in the United States, causing more than half a million deaths[1]. Cancer is a complex disease and the hallmark of cancer is hyper proliferative cells, which have evaded the cellular death pathways (cellular apoptotic machinery). In cancer, a group of abnormal cells divide uncontrollably beyond the normal limit, subsequently intruding the neighbouring tissues and distant organs (metastasis)[2, 3]. There are more than 100 types of cancers derived from various tissues and organs. Each cancer type is a result of various genetic and epigenetic alterations [4, 5]. Moreover, DNA damage caused by natural processes or by genotoxic agents has been correlated to be the causative agent for several diseases including cancer[6]. Cancer treatment may include chemotherapy, radiation, immunotherapy and/or surgery. However, chemotherapy remains one of preferred treatment of choice, involving various natural and synthetic compounds that have potential to kill or check the unwanted cancer cell growth. The discovery and the use of metal-based drugs offers much promise for cancer chemotherapy, which gained momentum after the serendipitous discovery of cisplatin by Barnett Rosenberg in 1960, is being clinically used for the treatment of solid malignancies[7]. Among the 4000 plus Platinum drugs tested as promising anticancer agents, only cisplatin, carboplatin and oxaliplatin are approved worldwide and the other three, nedaplatin, lobaplatin and heptaplatin (Fig. 1) have clinical approval in Japan, China and South Korea, respectively[8,9]. Nevertheless, the issues of systemic toxicity, drug resistance and limited therapeutic window have motivated researchers to look for targeted cancer therapies which involves the use of drugs or other compounds against the specific biomolecules like enzymes, proteins, DNA/RNA and cancer specific pathways involved in cancer cell growth[10-14].

P53 is an important cellular gene and is a well-studied transcription factor. p53, commonly referred as “guardian of the genome”, is a tumour suppressor protein whose primary function is to maintain cellular homeostasis and is activated upon cellular stress[15, 16]. It protects cells from several genotoxic challenges like hypoxia, free radicals, DNA damage, and UV light[17]. Upon DNA damage, p53 elicit a multifaceted response in the cell and it decides various important cellular processes like DNA repair, cell cycle arrest and apoptosis, thereby maintaining the genomic integrity of the cells[18, 19]. Unlike, other cellular transcription factors, p^{53} is known to be mutated in almost all types of cancer. Around 50% of human cancers have mutation in p^{53} gene suggesting its importance in cancer biology. P^{53} also plays important role in response to the several chemotherapeutic agents[20]. In response to widely used Platinum drugs like cisplatin and oxaliplatin, p^{53} plays a deciding role in inducing cell-cycle arrest or apoptosis. Lack of p^{53} function is also linked to cisplatin resistance[21, 22]. Moreover, p^{53} has also emerged as an attractive drug target which has led to recent discoveries of several small molecules targeting p^{53} and some are in clinical trials[23, 24].

Improving the design of metal-based drugs devoid of undesirable side effects and having different mechanism of action is a real challenge to the scientific community. In recent years, several transition metal-complexes have been investigated as purposive and apt alternatives to platinum-based drugs[25]. A plenty of Schiff base metal chelates currently known are recognized as potential pharmacological agents and have received considerable attention in the field of medicine [26]. Metal complexes including Iron (Fe), Cobalt (Co), Nickel (Ni), Copper (Cu), Zinc (Zn), Gold (Au), and Palladium (Pd) have displayed promising results in cancer therapy[27-29]. Cu is a nontoxic endogenous essential element. Its complexes have attained special interest as they trigger apoptotic cell death by stimulating proapoptotic proteins or antiapoptotic proteins[30-32]. The redox metal Cu has potential to generate ROS that brings about the oxidative damage of biomolecules like proteins, lipids, DNA and RNA. Hence a conceivable strategy is

to develop robust metal complexes of cheaper transition metals as new anti-cancer chemotherapeutics[33].

In continuation of our work on the design and synthesis of targeted metal based chemotherapeutic antitumor agents[34], we herein report the synthesis of Cu, Ni, and Co complexes from a Schiff base ligand (SB) derived from the condensation reaction of 2-hydroxynapthaldehyde with 1, 4-benzodioxan-6-amine. These metal complexes were investigated for their in vitro anticancer activity against human cervical (HeLa) and human keratinocyte (HaCaT) cancer cell lines. DNA binding potential were assayed using spectroscopic methods. In addition, ROS generation, cell cycle analysis, DNA damage assay, apoptotic pathway analysis (caspase-3 assay) and molecular docking studies were carried out to support the results of cancer cell cytotoxicity. Since, DNA is not always the primary target of metal based anticancer molecules[35, 36], we also explore the ability of these metal complexes to bind an important cellular transcription factor protein, p53, which is an important regulator of cell growth and cell death pathways[19-21]. Our molecular docking results suggest that the ligand binds to the central, highly conserved DNA-binding domain region of p53 (p53DBD), that could further activate the cancer cell DNA damage, which in turn could trigger the cell signalling pathways leading to cancer cell death.

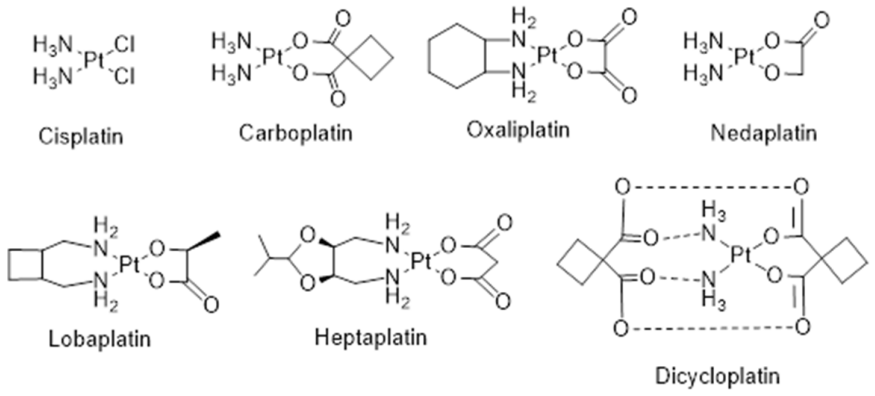

Fig. 1. Molecular structures of some platinum anticancer drugs that are approved or undergoing clinical trials.

2. Results and discussion

2.1. Chemistry

The condensation of 2-hydroxynaphthaldehyde with 2,3-Dihydro-benzo [1,4] dioxin-6-ylamine in a 1:1 molar ratio in methanol with a catalytic amount of acetic acid at room temperature resulted in the formation of the ligand (**SB**) (Scheme S1 in SI). The metal complexes **C1-C3** were obtained by the reaction of the ligand with corresponding metal salts in a 2:1 (L:M) molar ratio in methanol (See Scheme S1 in SI). The complexes obtained were non-hygroscopic solids, stable at room temperature, and soluble in $CHCl_3$, DMF, and DMSO. All the compounds were characterized by elemental analyses, ^{1}HNMR, ^{13}CNMR, FTIR, ESI-MS and UV-Vis spectral methods. Molar conductance values of the complexes (**C1-C3**) in 10^{-5} M DMSO solutions at room temperature were 23 $\Omega^{-1}cm^2mol^{-1}$, 18 $\Omega^{-1}cm^2mol^{-1}$ and 20 $\Omega^{-1}cm^2mol^{-1}$, respectively suggesting the complexes are neutral in nature. The physiochemical data of all the synthesized complexes and the free ligand is given in Table **1**.

Table 1. Physicochemical properties of the ligand (**SB**) and its complexes (**C1-C3**)

Compound	Color	Mol. Formula	Yield (%)	Mol. Wt.	Mp (°C)	Λ_m ($\Omega^{-1}cm^2$ mol^{-1})	μ_{eff} (BM)
SB	Yellow	$C_{19}H_{15}NO_3$	88	305.11	121	-	-
C1	Light green	[$C_{38}H_{28}CuN_2O_6$]	53	671.12	222	23	1.52
C2	Dark green	[$C_{38}H_{28}NiN_2O_6$]	48	666.13	227	18	2.82
C3	Brick red	[$C_{38}H_{28}CoN_2O_6$]	43	667.12	212	20	3.37

The FTIR spectra of the free ligand (**SB**) clearly shows a sharp peak due to ν(C=N) at ca. 1633cm^{-1} which favours the condensation reaction and confirms the successful synthesis of

the ligand (Fig. S2 in SI). In the complexes (**C1–C3**), the ν(C=N) vibration shifted to a lower frequency by ca. 6–19 cm^{-1}. The difference in the stretching C–O vibration bands (ca. 230 cm^{-1}) confirms the bidentate coordination of the ligand with the metal ion. Furthermore, coordination through the azomethinic nitrogen (M-N) and the phenolic oxygen (M-O) was supported by the appearance of additional new bands in the region 560-430 cm^{-1} (See Fig. S1-S4 in SI). The ESI mass spectra of the ligand (SB) and all the complexes (**C1–C3**) displayed molecular ion peaks at m/z 328.09, 671.12, 666.13 and 667.12 assignable to the corresponding $[M+Na]^+$ and $[ML]^+$ ions, respectively (see Fig. S5-S8 in SI).

^{1}H-NMR spectrum of the ligand (**SB**) gave reasonable peaks which are in accordance to the structure of the compound. A peak at approximately δ 9.59 ppm attributed to the azomethinic hydrogen (-CH=N-) while the peak at approximately δ 15.90 ppm may be assigned to the hydrogen of the hydroxyl groups attached to aromatic ring. Meanwhile, the spectrum does not display a peak due to NH_2 protons, thus supporting the successful synthesis of Schiff base ligand. Likewise, the sharp signal at δ 4.29 ppm has been assigned to the two equivalent CH_2 groups, respectively. The aromatic protons are observed in the range δ 6.94-8.52 ppm. The ^{13}C NMR spectrum of the ligand (**SB**) showed the imine carbon (C= N) peak at 170.05 ppm. The aromatic carbons were observed at 155.80-109.46 ppm and the aliphatic CH_2 carbons were recorded at 65.09 ppm, respectively. The ^{1}H-NMR and ^{13}C-NMR spectrum of the Schiff base (SB) ligand is given supporting information (See Fig. S9 and S10).

The electronic absorption spectra of the free ligand (**SB**) and its complexes (**C1-C3**) in 10^{-5} M DMSO (Experimental section) show peaks in the UV region at 245, 277 and 345 nm which are attributed to π → π* and n→ π*transitions of the free Schiff base ligand. In addition, the broadbands observed in complexes at 436 and 423 nm (**C1** and **C3**) and 362 nm (**C2**) are assigned to the ligand-to-metal charge transfer transition. The UV-Vis. spectrum of complex **C1** displayed aband at 576 nm assigned as a $^2B_{1g}\rightarrow {}^2E_{1g}$transition, confirming the square planar

geometry around the copper(II) ion. In complex **C2** and **C3** the absorption bands at 595 and 603 nm are assigned to $^3T_1(F) \rightarrow {}^3T_1(P)$ and $^1A_{1g} \rightarrow {}^1B_{1g}$ transitions respectively supporting a tetrahedral geometry for **C2** and a distorted square planar geometry for **C3** [37, 38]. The electronic spectra of the ligand and the complexes are given in figure **2**. Besides the observed magnetic moment of the complexes are 1.52 BM for **C1** and 3.57 BM for **C3** suggesting a square planar geometry around the metal ions. The observed magnetic moment of **C2** was found to be 2.82 BM indicating the complex has a tetrahedral structure [38].

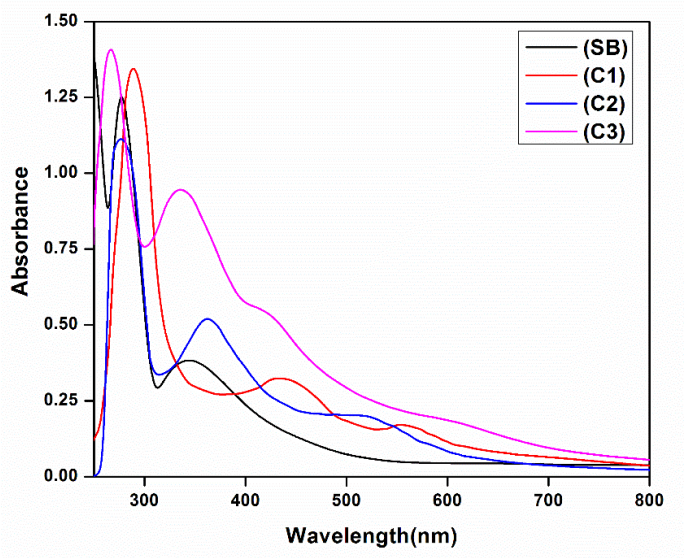

Fig. 2. Electronic spectra of the ligand (SB) and metal complexes **C1-C3**.

Thermal analysis of the complexes (**C1-C3**) was carried in the temperature range of 40- 800 ^oC by using thermo gravimetric technique at a heating rate of 10 ^oC/min. In complex **C1** the decomposition occurs in two stages. The first stage proceeded with the weight loss of 43% (calcd. 44.4 %) in the temperature range of 222-395^oC which may be attributed to the loss of $C_{16}H_{14}N_2O_4$ group. The second decomposition step continued with the weight loss of 45% (calcd. 46.25%) in the temperature range of 400-700^oC. This weight loss is due to the loss of $C_{22}H_{14}O_2$ group. The overall weight loss observed in **C1** was found to be 89% (calcd. 90.65%).

The metallic Cu left as the residue has the observed weight of 9.6% against the calculated value of 9.47%. The complexes **C2** and **C3** displayed similar decomposition steps with slight variations in decomposition temperatures. The TG curves of the complexes (**C1-C3**) are given in Fig. S11 in SI.

2.2. Crystal Structure and XRD

Single crystals for the ligand **SB** were obtained readily but all attempts to obtain the crystals of the metal complexes failed. Therefore, the ligand was structurally characterized by X-ray crystallography and X-ray powder diffraction studies were carried out for the complexes to determine whether the complexes are crystalline or amorphous in nature. The ligand (**SB**) crystallizes in an Orthorhombic system with a space group of P n a 21 (Fig. **3**). The crystallographic data of the ligand (**SB**) and other structural refinement parameters are provided in Table T1 (See SI) and the selected bond distances and main bond angles are given in Table T2 (See SI). The azomethinic bond, N1-C6, 1.275(8) Å is in agreement with a formal -C=N- double bond and the O3-C15 bond length of 1.324(10) Å, is somewhat shorter than the normal C-O single bond. The bond length for N1-C7, 1.412(9) Å and C5-C6, 1.420(10) Å for the ligand is nearer to N-C and C=C bonds lengths, respectively. The unit-cell packing diagram of SB displayed hydrogen bonding interaction between the nitrogen of azomethinic group and the hydroxyl hydrogen atom. The single crystal X-ray diffraction study revealed that the Schiff base (SB) exhibits an imine-ol form (See Figure 3(A) and (B) and Figure **S12** in SI).

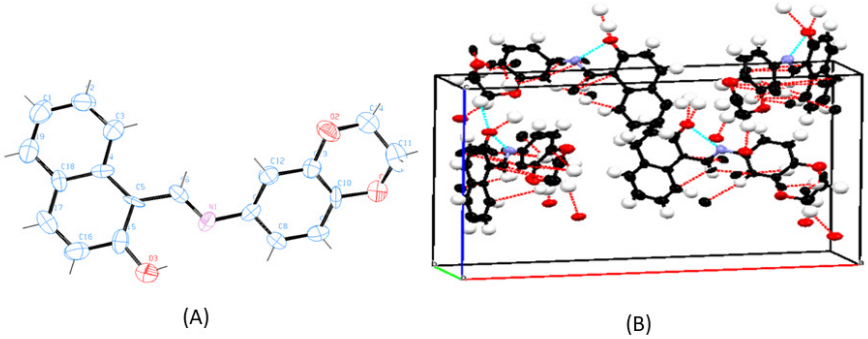

Fig. 3. (A) ORTEP diagram of the ligand **SB** with thermal ellipsoids drawn at the 50% probability level. All hydrogen atoms are shown with single bonds radiating from the atoms for the sake of clarity. (B) Unit cell packing diagram of the ligand SB with hydrogen atoms showing hydrogen bonding and short contacts.

The powder XRD of the complexes were carried out in the range 10-70^{o} (θ) at a wavelength of 1.54 Å. The different XRD pattern indicates that the complexes **C1-C3** have well defined crystalline patterns with various degrees of crystallinity, as shown in **Fig. 4**.

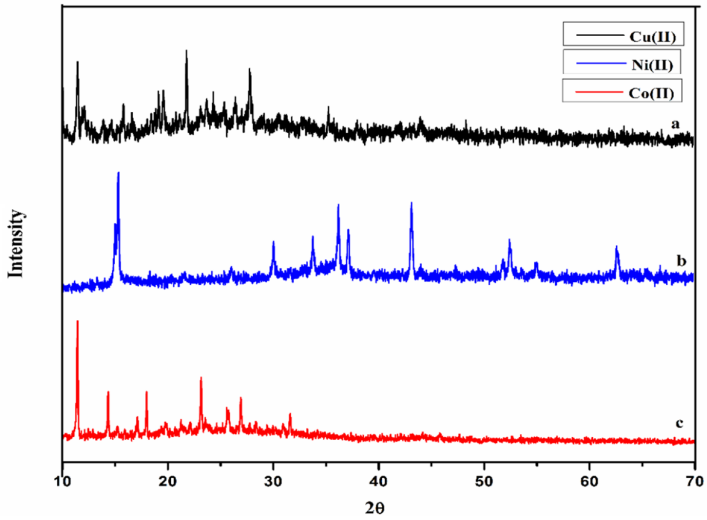

Fig. 4. Powder X-ray diffraction pattern of (a) **C1,** (b) **C2** and (c) **C3** complex.

2.2.Biology

2.2.1. Metal complexes inhibited human cancer cell growth

The efficiency of metal complexes in suppressing cell growth and engendering apoptosis has been well documented [39, 40]. The *in vitro* cell culture studies provide valuable information for

the screening of chemotherapeutic agents and preliminary data for further relative studies. Thus, cytotoxicity (**Fig. 5; Table 2**) of complexes **C1–C3** against two different human cancer cell lines, viz. HaCaT (human keratinocyte) and HeLa (human cervical) cancer cells, were evaluated through the loss of cell viability using the colorimetric MTT (3-(4,5-dimethylthiazol-2-yl)-2,5-diphenyltetrazolium bromide) assay. The cells were treated with the complexes (**C1-C3**) for 24 h and 48 h, respectively. A dose-dependent antitumor activity of **C1-C3** was observed in both the cancer cells. Complex, **C1** exhibited significant cytotoxicity against the HeLa cancer cells with an IC_{50} value of 17.65 μM (incubated for 24 h), 9.05 μM (incubated for 48 h) and is more potent than the widely used drug cisplatin (IC_{50} = 27.2 ± 1.71 μM) under similar experimental conditions[34]. This is in accord with the DNA binding propensity order of complexes **C1–C3** (as mentioned below). Since the *in vitro* cytotoxicity was found to be the highest for cervical cell line (HeLa cells) among our complexes and that cervical cancer is one of the most common cancer in women[41] we preferred to use this cell line for all further studies.

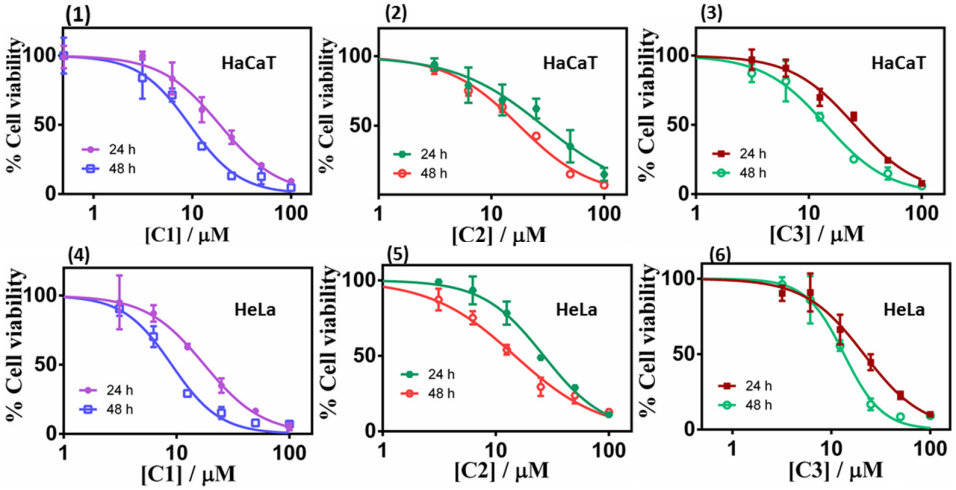

Fig. 5. Cell viability plots (1)-(3) and (4)-(6) showing cytotoxicity of the respective complex C1–C3 in HaCaT and HeLa cells incubated for 24 h and 48 h respectively.

Table 2. IC_{50} values of the complexes (C1–C3) against HeLa and HaCaT cancer cells.

Compounds	Incubation time (24 h) IC_{50} (μM)		Incubation time (48 h) IC_{50} (μM)	
	HeLa	**HaCaT**	**HeLa**	**HaCaT**
C1	17.65	19.01	9.05	9.38
C2	26.58	28.95	14.78	17.69
C3	21.35	25.35	13.41	14.17

2.2.2. Absorption spectroscopic studies of the Interaction between DNA and complexes

Absorption spectroscopy is one of the most useful and effective techniques in DNA-drug interaction studies. This technique allows recognizing the existence of interactions between DNA and molecules, as well as specifying the mode of interaction by utilizing the perturbations in the spectral observation[19, 42, 43]. Binding of different compounds to DNA may create a strong stacking interaction between the compounds and the base pairs of the DNA, and may cause the absorbance spectrum show some degrees of hypo- or hyperchromism[43]. The interaction of synthesized compounds with Ct-DNA may occurs by three different modes of binding which includes (i) Electrostatic binding / External binding, (ii) Groove binding, (iii) or Intercalative binding/Intercalation. In our studies, electronic absorption spectroscopy was used to determine the binding capacity and the mode of interaction of the synthesized compounds with Ct-DNA, displaying characteristic absorbance changes and wavelength shifts (**Fig 6**). The absorption spectral changes on addition of increasing concentrations of Ct-DNA to the fixed concentration solution of the compounds was observed. It is known that upon the binding of Ct-DNA with the metal complexes, an evident "hypochromic shift" occurs in the absorbance of the ligand centred band[34]. On increasing Ct- DNA, all the metal complexes exhibited a hypochromic and a slight red-shifted (bathochromic shift) band in the absorption spectra. The hypochromic values observed in the presence of DNA were in the range 4.06– 15.95%, and their red shifts

are by 1-3 nm. The presence of hyperchromism indicates the formation of complex between DNA and the metal complexes[34]. The intrinsic binding constant K_b calculated from the plots of [DNA]/(εa- εf) verses [DNA] was obtained from the ratio of the slope to the intercept (please see methods). Using the hypochromic shifts, the intrinsic binding constant K_b for DNA binding by the ligand **SB** and the metal complexes **C1, C2** and **C3** were determined to be 2.84×10^5, 1.97×10^5, 1.35×10^5 and 1.22×10^5 M^{-1} respectively. These studies indicate that all the three metal complexes have binding constant in the similar range indicating a similar mode of binding to the CT-DNA[34]. However, complex **C1** showed higher binding affinity towards the CT-DNA followed by **C2** and **C3**. These results suggest the binding of compounds to the CT-DNA. Since, the apparent binding constants of the compounds are in the range of 10^5 M^{-1} it can be predicted that these complexes bind to the DNA in an intercalation mode[34, 44-46]. The exceptionally high value of K_b for the compound **C1**, advocates the complex is an ardent binder of DNA. Since such high binding constant is generally characteristic of DNA binding by intercalation, so we undertake that the ligand **SB** and complexes **C1, C2** and **C3** bind DNA mainly by intercalation, however electrostatic interactions, H-bonding as well as interactions with the negatively charged phosphate groups of DNA may also offer their role towards overall binding strength[34, 46]. (See detail below in Docking study).

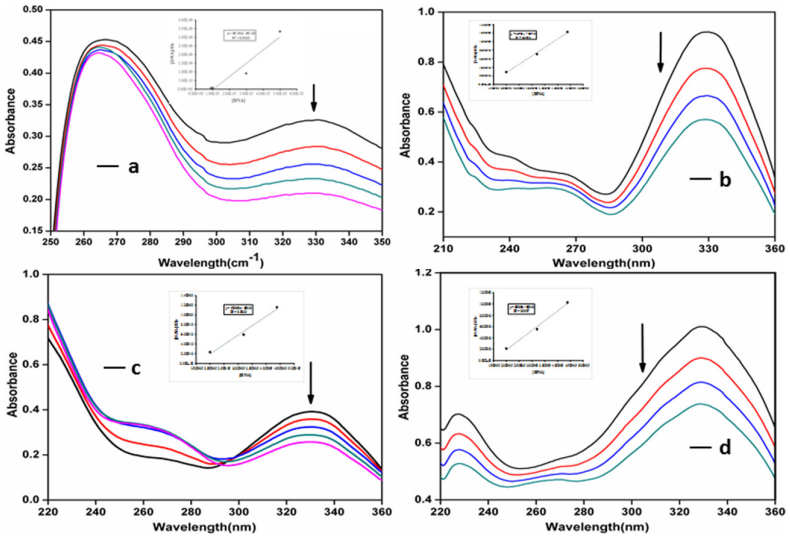

Fig. 6. Absorption spectra of the ligand **SB** (a) and complexes **C1** (b), **C2** (c) and **C3** (d) in the presence of increasing amounts of Ct-DNA at room temperature in 5 mM Tris-HCl/NaCl buffer (pH = 7.4) at 25°C. The arrow shows the absorbance changing upon increasing the DNA concentration. The plots of [DNA]/εa – εf) versus [DNA] for the ligand and the complexes are shown as insets in respective graphs (a), (b), (c) and (d).

2.2.3. Nuclear Morphology Study

Changes in the morphology of the nucleus is an important feature of cell death. Condensed chromatin and fragmented nucleus are the distinguishing feature of the apoptotic cell death. To determine the effect of complexes on the nuclear morphology and nature of cell death (apoptosis or necrosis), DAPI staining was used upon the treatment of compounds (**C1-C3**). As shown in Fig.**7A**, in control cells, a uniform level of blue fluorescence in the nucleus was seen which specifies that nearly all cells are alive and healthy. However, upon treating the cells with 15 µM complexes (**C1-C3**), morphological changes in the nucleus can be observed. In the complex treated cells, fragmented nuclei were observed suggesting the presence of apoptotic bodies[47]. Treatment with compounds for 24 h (15 µM), **C1-C3** shows about 36%, 25% and 24% apoptotic cells, respectively (Fig. **7B**). Results obtained from stained cells, showed a significant higher percentage of compound **C1** treated cell undergoing apoptosis. In our case, we have seen apoptotic cells instead of necrotic feature of cells upon long exposure (data not

shown). Our data suggests that complexes (**C1-C3**) drive the cells through apoptotic mode of cell death in HeLa cells.

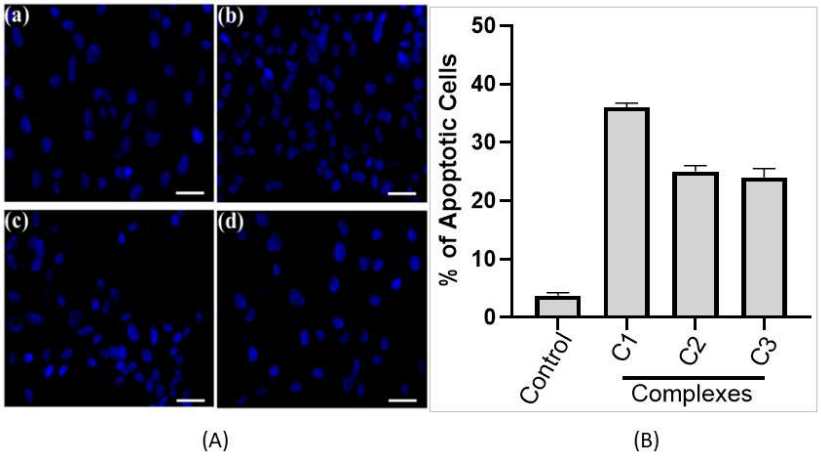

Fig. 7(A) Metal complexes induce cancer cell apoptosis. Florescence images of cervical cancer (HeLa) cells displaying morphological changes; (a) in absence of complexes (control) and on exposure to complexes (b) C1 complex, (c) C2 complex and (d) C3 complex detected with DAPI (blue) staining. Arrows indicate apoptotic nuclear fragmentation. Experiment was performed three times. **(B)** Representative figure is shown. Scale bars, 10 μm. (e) Bar graph represents the percentage of apoptotic cells determine by DAPI staining. Value represents the mean ± SD, n = 3.

2.2.4. Intracellular reactive oxygen species (ROS) production is involved in metal-complex induced apoptosis.

ROS is known to play an important role in activating the cell death pathways. Such chemical species are not only produced under pathological conditions but also during physiological conditions like cellular metabolic processes. Various studies have shown that ROS damages DNA, RNA and also bring about the oxidation of proteins and lipids. To study the impact of metal complexes on oxidative stress, intracellular ROS production in compound treated HeLa cells was measured by DAFH-DA (2′,7′-dichlorofluorescein diacetate), a non-fluorescent membrane permeable probe, which oxidizes in the presence of peroxides to the highly fluorescent DCF (2′,7′-dichlorofluorescein)[43]. As shown in Fig. **8**, the ROS levels generated in response to 15 μM (24h) of compounds (**C1-C3**) treatments were significantly higher than

control cells. Interestingly, ROS generated by **C1** was significantly higher than **C2** and **C3**. These results suggest that the complexes **C1-C3** may induce apoptotic pathways mediated by ROS.

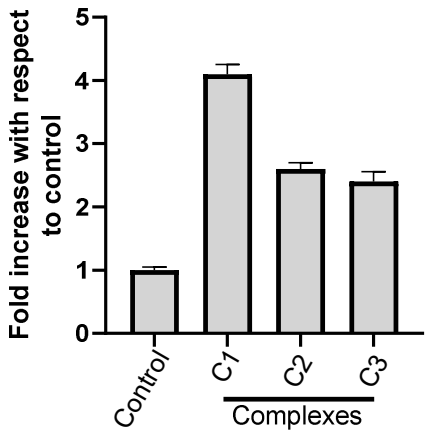

Fig. 8. Determination of intracellular ROS level (DCF-DA assay) in human cervical cancer cell line HeLa, treated with solvent control and with different complex C1, C2 & C3 at 15μM; each for 24h. Results are expressed as fold increase with respect to control. Each value represent mean ± SD, of five independent experiments.

2.2.5. Metal complexes induced DNA oxidation and DNA damage in HeLa cells

DNA damage is a natural phenomenon happening in all cells in daily life of a cell. Most of the DNA damage happens by DNA oxidation which leads to the formation of different lesions including oxidized bases, apurinic/apyrimidinic (AP) sites, and DNA single- and/or double-strand breaks. Oxidation of guanine base is more common as compared to other DNA bases mainly due to its low oxidation potential[48, 49]. 8-hydroxy-2′-deoxyguanosine (8-oxo-dG) is the most common form of oxidized guanine and hence is a good indicator for measuring DNA oxidation[48, 49]. Increased levels of ROS in metal complexes treated HeLa cells may cause DNA damage. Hence, to explore the effect of metal complexes on DNA oxidation DNA damage, production of 8-oxo-dG was evaluated. Cellular 8-Oxo-dG formation was examined using 8-Oxo detection ELISA kit (see methods). As shown in (Fig. **9**), treating HeLa cells for 24 h with

increasing concentration of metal complexes have resulted in increased formation of 8-oxo-dG in the genomic DNA for all the three complexes. As expected, complex **C1** produced more 8-Oxo-dG as compared to **C2** and **C3** which is consistent to the higher generation of ROS by complex **C1** than **C2** and **C3** (Fig. **8**). These results indicate that the ROS generated by metal complexes are tightly correlated with DNA damage and DNA binding. Moreover, these results are also in agreement with the nuclear morphological studies (Fig **7**).

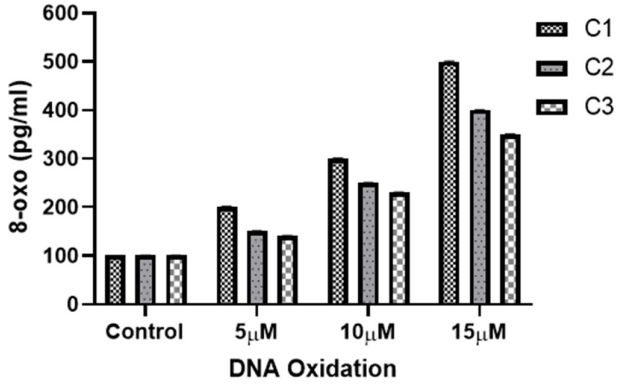

Fig. 9 Determination of 8-oxo-dG of HeLa cells genomic DNA. HeLa cells were incubated with increasing concentrations of metal-complexes for 24 h and the amount of 8-oxo-dG formation was assessed using ELISA kit (see methods). Each value represent mean ± SD, of three independent experiments.

2.2.6. Cell Cycle Analysis

Cell cycle progression is impaired by DNA damage. Also, our results have shown the antiproliferative role of complexes in HeLa cells. Thus, we next analysed the cell cycle of HeLa cells after incubating the cells with respective complexes with 15 μM for 24 h. Fig.**10** shows the distribution of cells in different phases of cell cycle. As the FACS analysis showed, treatment with HeLa cells with the complexes significantly increased the cell population in the SubG0 phase as that of control (4.5% in control, 30.3% in **C1**, 19.3% in **C2** and 19.7% in **C3** treated cells), which shows the apoptotic cell population. However, treatment of metal

complexes led to a decrease in G0/G1 cell population (60.5% in control, 43.1% in **C1**, 52.1% in **C2** and 52.5% in C3 treated cells), and which is more prominent in the **C1** treated cells (Fig. **10**). A slight decrease in S phase cell population was also observed for all complex treated cells.

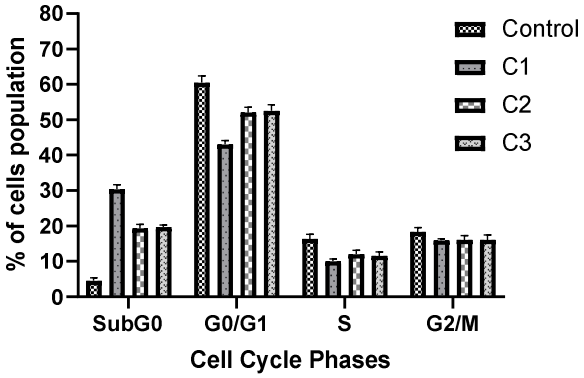

Fig. 10. Metal complexes induce apoptosis in HeLa cancer cells. Cell cycle analysis was performed upon treatment of cells with 15 μM of metal complexes for 24 hours. After fixation, cell cycle analysis was performed with propidium iodide staining. Bar graph represents the percentage of cell population in different phases of cell cycle. Value represents the mean ± SD from three independent experiments.

2.2.7. Metal complexes-Increased Caspase-3 Activity in HeLa Cells

Caspase-3 enzyme is a crucial mediator and an important upstream factor of programmed cell death (apoptosis). Activation of caspase-3 leads to apoptosis[50, 51]. Our cell cycle analysis and nuclear morphological studies has established the occurrence of cell death by apoptosis upon metal complex treatment. Hence, we investigated the effect of metal complexes on caspase-3 activation. The caspase-3 enzyme activity was analysed spectrophotometrically. It was found that the complexes **C1**, **C2** and **C3** treatment (15 μM) for 24h increased caspase-3 enzyme activity in HeLa cervical cancer cells (Fig **11**) as compare to control. However, **C1** treatment resulted in a significantly higher ($p < 0.05$) caspase-3 activity than **C2** and **C3**. These results strongly suggest the involvement of caspase-3 in the complex-induced apoptosis.

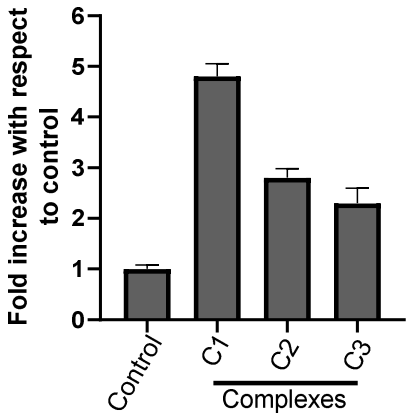

Fig. 11. Effect of metal complexes on caspase-3 activity in HeLa cells. Cells were treated with solvent control and with different complex C1, C2 & C3 at 15µM; each for 24h and cytosolic extracts were used for caspase-3 activity. Results are expressed as fold increase with respect to control. Each value represent mean ± SD, of three independent experiments performed in duplicate.

2.2.8. Molecular Docking Studies

Based on our spectroscopic and cell culture-based studies we found that compound **C1** to be a better candidate against the cancer cells, hence, we performed the molecular docking studies using the promising lead compound **C1** and **SB** to the DNA molecule. Molecular docking experiments of complex **C1** and **SB** were carried out with DNA duplex of the sequence d(CGCGAATTCGCG)2 dodecamer (PDB ID: 1BNA) in order to predict the preferred orientation of the complex inside the DNA helix and to substantiate the spectroscopic results[52]. 2D structure of the synthesized ligand molecules were converted to energy minimized 3D structures and used for docking studies. DNA duplex of sequence d (CGCGAATTCGCG)2 dodecamer was taken as the target receptor. The Lamarckian genetic algorithm, inculcated in the docking program AutoDock 4.2, was employed to satisfy the purpose. Crystal structure was obtained from Protein Data Bank (https://www.rcsb.org) with the PDB ID 1BNA. Molecular docking calculations werecarried out with Auto dock vina[53]. The conformation with the lowest binding free energy was used for analysis. All molecular docked models were prepared using

PyMOL viewer. Docked images are shown in Fig. **12**. On analysing the docked structures, it is evident that the ligand and its metal complex **C1** fit well into the A-T rich region of target DNA. Both **SB** and **C1** are stabilized in the A-T rich region through various interactions, such as van der Waals and hydrophobic interactions. Binding affinity values of the docked target compounds were found to be in the range of −12.6 to −10.1 kcal mol−1.)

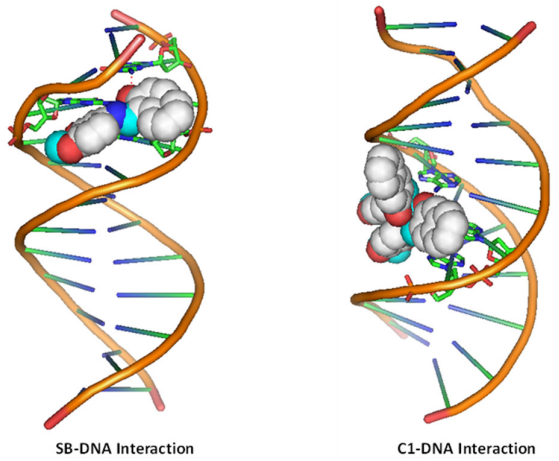

Fig. 12. Docking study of the binding of SB and C1 to DNA.

Our data shows that metal complex **C1** induces DNA damage by binding to the DNA molecule, inhibits cell growth and further causes cell death. Owing to the importance of p53 transcription factor in regulating cellular stress, DNA damage repair function along with its pivotal role in deciding cell death and survival, we intended to investigate the ability of **C1** in binding the p53. P53 mediates most of its function though binding to the DNA molecule. Therefore, we looked into the effect of compound **C1** and ligand **SB** on the p53 binding ability to the DNA using molecular docking studies. Crystal structure of the p53 complexed with DNA molecule[54] was obtained from Protein Data Bank (https://www.rcsb.org) with the PDB ID 1TSR (see methods for detail). Figure **13** shows that p53DBD interacts with DNA via LYS120, SER241, ARG273, ARG280, and ARG281 residues. However, unlike the strong interaction of both SB

and C1 with DNA (Fig. **12**), we observed that complex C1 goes inside the p53DBD pocket but doesn't show any remarkable interactions with DNA (data not shown). This could be because the complex undergoes de-metalation inside the cell and the ligand is actually responsible for the biological activity[55, 56]. This presumption however demands more mechanistic studies and other factors such as cellular environment which can affect the metal complexes by redox pathways, ligand exchange, expansion or contraction of the coordination sphere with the change in pH, among others, cannot be ruled out. In this study, we found that the Cu based metal complex **C1** showed interesting anticancer property which could be related to the potential of copper to form tetrahedral, square planar and distorted octahedral complexes. Once inside the cell a copper complex can change its geometry, undergo ligand exchange or a one-electron reduction of Cu(II) to Cu(I) in a hypoxic environment could release the ligands as has been observed in some Co(III) and Cu(II) complexes[57, 58].

Interestingly, we found that the ligand SB binds the same DNA binding pocket of p53DBD and thus mimicking similar interactions as that of p53DBD and DNA. SB fits the binding pocket of p53DBD where it makes contact with critical residues SER241, ARG273 and VAL274 of p53DBD which are also responsible to bind DNA (Fig. **13**). Importantly, both the DNA and the SB share residues SER241 and ARG273 of p53DBD, further suggesting a common binding pocket for both SB and DNA (Fig.**13**). Therefore, we presume that binding of SB will block or disengage the p53 binding to the cognate DNA binding sites and thus negatively affect p53 DNA repair function and other DNA stress responses mediated by p53.

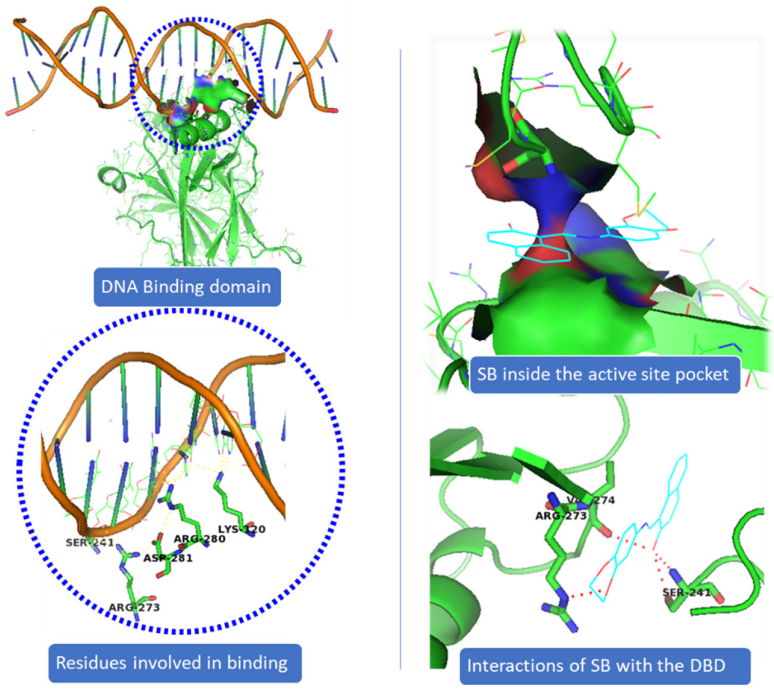

Fig. 13. Docking study of the binding of SB to the p53DBD. P53 DBD shows interaction via LYS120, SER241, ARG273, ARG280, and ARG281 whereas, SB shows interaction with SER241, ARG273 and VAL274 inside the same binding pocket.

2.2.9. Implications of metal-complexes in Cervical Cancer Treatment

Cervical cancer is the fourth most frequent cancer in women with an estimated 570,000 new cases in 2018 representing around 7% of all female cancers. Diagnosing of cervical cancer at an early stage and providing access to effective treatment can significantly improve the likelihood of survival (WHO report). While the diagnosis of advanced, recurrent, or persistent disease is often incurable. Chemotherapy based treatment in cervical cancer is mainly cisplatin-based. However, reports of the use of new metal complexes against cervical cancer are also available[28].

Since our data is primarily based on Hela cell, which is derived from cervical cancer, we believe that our results will have an important implication for the treatment of cervical cancer. It is worth noting that unlike most of the cancers, p53 is not mutated in HeLa cells (cervical cancer

derived cells). Most of the tumor-related p53 mutations, called hotspot mutations, occur in the DNA-binding core domain (p53DBD) of p53. ARG273, an important DNA-contact amino acid, is one of the most frequently altered amino acid residues in human cancer [59]. However, p53 ARG273 is not mutated in cervical cancer, a residue also important for the binding of ligand, SB and that would negatively impact p53-DNA binding. Mechanistically, we believe that binding of the metal complex, namely, **C1** and ligand **SB** to the DNA causes the DNA damage which inturn will attract DNA repair protein, p53. Similarly, binding of **SB** to the p53DBD will inhibit the normal DNA protective functions of p53 and could lead to further increase in DNA damage. The inability of **SB** bound p53 to mediate the DNA repair pathway will lead to increased destabilization of the cellular genomic DNA due to increase in DNA damage and lack of p53 function, that could trigger apoptosis mediated cell death, as we observed in this work. P53 regulate the apoptotic processes at various levels by regulating several proapoptotic proteins. In our experiments, we found the induction of apoptotic hall mark protein, caspase-3 upon treatment with metal complexes[60-62]. A higher level of caspase-3 induction by complex **C1** could be positively attributed to a higher level of ROS and the subsequent DNA damage generated by compound **C1** (Fig **8** and Fig **9**) which was significantly higher than compound **C2** and **C3**. Our results are also in agreement with other reports of metal complexes inducing apoptosis via caspase-3 pathway[63-65].

3. Conclusions

In conclusion, through the present work new heterocyclic Schiff base complexes (C1–C3) have been described. Various physicochemical techniques supported the successful formation of the compounds. The complexes exhibit *in vitro* cytotoxic activity against human keratinocyte (HaCaT) and human cervical cancer (HeLa) cell lines, with the potency of C1, being even higher than that of the widely used drug cisplatin (IC_{50} = 27.2 ± 1.71 μM) against the human cervical cancer (HeLa) cell line. The antiproliferative activity of complexes (C1-C3) was

further proved by nuclear morphological staining and ROS studies. Complex **C1** can not only inhibit the proliferation of the HeLa cancer cell line, but also induce apoptosis. Furthermore, absorption studies demonstrated that the complexes effectively bind to DNA through an intercalative mode, in the order of SB > C1 > C2 > C3. These complexes, particularly the copper complex **C1** presented herein exhibits considerable biological activity and the studies can contribute to the rational design of novel potential anticancer agents.

4. Experimental section

4.1. Materials and physical methods

The reagents used in the syntheses of the ligand and transition metal salts were obtained from commercial sources and used as received without further purifications. Solvents were dried and distilled prior to their use following standard procedures. 3-(4,5-Dimethylthiazol-2-yl)-2,5-diphenyltetrazolium bromide (MTT) was purchased from Hi-Media. Calf Thymus (CT) DNA was purchased from Bangalore Genie (India). The elemental microanalyses of the synthesized compounds were performed at centre instrumentation facility, Jamia Millia Islamia using Elementar (Thermo Scientific) CHN Elemental analyzer. ^{1}H- (400 MHz) and ^{13}C- (100 MHz) NMR spectra were run on a Bruker spectrometer using tetramethylsilane [$Si(CH_3)_4$] as the internal reference. IR and electronic absorption spectra were recorded on a Bruker Alpha Fourier transform infrared (FT-IR) spectrometer and a Perkin-Elmer LAMBDA 40 UV/visible spectrophotometer, respectively. Molar conductance values of the complexes were obtained using a type 305 Systronic conductivity bridge in DMSO solution. Electrospray ionization mass spectrometric data (ESI-MS) were acquired in methanol on a Bruker Micro TOF QII, and a Thermo Finnigan LCQ Advantage Max ion trap Mass Spectrometer. The magnetic susceptibility data of the synthesized complexes was obtained by using the Faraday balance. Powder X-ray diffraction patterns of all compounds were carried out at room temperature using XPERT-PRO, X-ray diffractometer using CuKα monochromatic radiation (λ = 1.5406 A^{o}) in

the range of $10° \leq 2\theta \leq 70°$. The thermogravimetric analysis (TGA) of the synthesized complexes was performed in the temperature range of 40-800 ^{o}C in a dynamic nitrogen atmosphere with a heating rate of 10 ^{o} C/min using Exstar 6300 Thermogravimetric analyzer.

4.2. Syntheses

Synthesis of 1-[(2,3-Dihydro-benzo[1,4]dioxin-6-ylimino)-methyl]-naphthalen-2-ol (SB). To a solution of 2-hydroxynaphthaldehyde (172 mg, 1 mmol) in dry methanol (5 mL) 1,4-Benzodioxan-6-amine (151 mg, 1 mmol) dissolved in dry methanol (5ml) was added in fractions, drop wise over 15 minutes and the reaction mixture was stirred for 4h at room temperature. Completion of the reaction was monitored by TLC and after that the solvent was removed under reduced pressure. The residue thus obtained was collected, dried and recrystallized in ethanol. Crystals suitable for X-ray diffraction were obtained after two days. Yield: 88% (0.27g) Color: Golden Yellow; M.P: 121 °C. Mol. Wt. 305.11, Anal. Calc for $C_{19}H_{15}NO_3$: C, 74.74; H, 4.95; N, 4.59. Found: C, 74.35; H, 4.87; N, 4.65. IR (KBr disc, cm^{-1}): 3430.25 (ph-OH), 1608.77 (C=N), 3055.16 (Aromatic C-H), 2880.40 (CH_2), 1485.16 (C=C), 1272 (C-O). Mass spectrum (ESI) $[M+Na]^+$= 328.09. UV -vis (DMSO): λ/nm 272, 352. ^{1}H-NMR (DMSO-d6, δ, ppm); 9.59 (1H, s, HC=N), 15.90 (1H, s, Ar-OH), 6.94–8.52 (m, Ar-H), 4.29 (4H, s, CH_2). ^{13}C-NMR (DMSO-d6, δ, ppm); 155.80 (CH=N), 144.96 (C-N), 170.05 (C-OH),143.38 (C-O), 109.46-138.76 (Ar C's), 65.05-65.09 (-OCH_2).

Synthesis of [Cu(SB)$_2$] (C1). To 10 mL yellow methanolic solution of SB (152 mg, 0.5 mmol), a methanol solution of $CuCl_2.2H_2O$ (43 mg, 0.25 mmol, 10 mL) was added dropwise with gentle stirring. One to two drops of triethylamine (20 μL) was added to the reaction mixture to adjust the pH to 7. The mixture was stirred for 3 h at room temperature resulting in the formation of light green precipitate which was filtered and dried in a vacuum desiccator. Several attempts of recrystallization didn't produce any crystals. Yield: 89 mg (53% based on

CuII salt). Color: Light Green; M.P: 222 °C. Mol. Wt. 671.12. IR (KBr disc, cm^{-1}): 1576, 2910, 1502, 1143, 547, 437. Elemental analysis (%): calc. for $C_{38}H_{28}CuN_2O_6$: C, 67.90; H, 4.20; N, 4.17. Found: C, 67.83; H, 4.36; N, 4.22. Mass spectrum (ESI) $[ML]^+$= 671.13. UV -vis (DMSO): λ/nm 289, 434, 576. Molar conductance (1.0×10^{-4} M; DMSO, $\Omega^{-1}cm^2mol^{-1}$): 23.

Synthesis of [Ni(SB)$_2$] (C2). Complex 3 was synthesized by a method similar to that of C1 and C2, using $NiCl_2.6H_2O$ (59 mg, 0.25 mmol) as the metal salt. Dark green precipitate was collected from the final reaction mixture which after filtration and several washings with cold methanol and diethylether was dried in a vacuum desiccator. Yield: 79 mg (48% based on NiII salt). Color: Dark Green; M.P: 227 °C. Mol. Wt. 666.13, IR (KBr disc, cm^{-1}): 1598, 2975, 1498, 1153, 545, 431. Elemental analysis (%): calc. for $C_{38}H_{28}NiN_2O_6$: C, 68.39; H, 4.23; N, 4.20. Found: C, 68.43; H, 4.13; N, 4.20. Mass spectrum (ESI) $[ML]^+$= 666.15. UV -vis (DMSO): λ/nm 276, 362, 515. Molar conductance (1.0×10^{-4} M; DMSO, $\Omega^{-1}cm^2mol^{-1}$): 18.

Synthesis of [Co(SB)$_2$] (C3). To 10 mL ethanol solution of SB (152 mg, 0.5 mmol) and $CoCl_2 \cdot 6H_2O$ (59 mg, 0.25 mmol) in the ratio of 2:1 (L:M), triethylamine (20 µL) was added dropwise under stirring to adjust the pH to 7. The mixture was stirred at room temperature for about 4 h. The resulting brick red precipitate obtained was filtered, washed several times with cold methanol and diethyether and then left to stand at room temperature for drying in a vacuum desiccator. Yield: 72 mg (43% based on CoII salt). Color: Brick Red; M.P: 212 °C. Mol. Wt. 667.12. IR (KBr disc, cm^{-1}): 1583, 2934, 1494, 1284, 547, 476. Elemental analysis (%): calc. for $C_{38}H_{28}CoN_2O_6$: C, 68.37; H, 4.23; N, 4.20. Found: C, 68.33; H, 4.24; N, 4.17. Mass spectrum (ESI) $[ML]^+$= 667.13. UV -vis (DMSO): λ/nm 267, 337, 603. Molar conductance (1.0×10^{-4} M; DMSO, $\Omega^{-1}cm^2mol^{-1}$): 20.

4.3. Crystal structure determination

Crystal suitable for single crystal X-Ray diffraction analysis were obtained on slow evaporation of an ethanolic solution of the ligand (**SB**) at room temperature. Selected crystal data of the ligand molecule (**SB**) is given in Table S1 and S2. X-ray diffraction data of the ligand (SB) was collected on a Bruker SMART CCD diffraction using graphite-monochromated Mo Kα radiation (k = 0.71073 Å) by u and x scans. X-ray data reduction structure solution and refinement were done using the SHEL XS-97 and SHELXL-97 packages[66]. The structure was solved by direct methods. Structural information for the compound has been deposited at the Cambridge Crystallographic Data Centre (CCDC).

4.4. Cell Culture

Human cervical cancer (HeLa) cells and the spontaneously immortalized human keratinocyte line HaCaT were maintained in complete Dullbecco's modified Eagle medium (DMEM) consisting with 10% fetal bovine serum (FBS) supplemented with 20 mM L-glutamine, 100 units per mL penicillin and 100 μg mL^{-1} streptomycin at 37 °C under a humidified atmosphere of 5% CO_2 [67].

4.5. Cell viability and proliferation assay/MTT assays

HaCaT and HeLa cell lines were used to determine the anticancer and cytotoxic activity in this study. Cell viability was checked by the MTT assay which is a colorimetric assay based on the conversion of the yellow tetrazolium salt MTT to purple formazan crystals after reaction with mitochondrial dehydrogenase of metabolically active cells. Stock solutions of the complexes **C1–C3** were prepared in DMSO and diluted with DMEM (Dulbecco's Modified Eagle's Medium) (the final concentration of DMSO did not exceeded 1% v/v). The cell lines were maintained in complete DMEM (a culture medium consisting 10% fetal bovine serum, supplemented with 20 mM L-glutamine, 100 units per mL penicillin and 100 μg mL^{-1} streptomycin) at 37 °C under a humidified atmosphere of 5% CO_2. Briefly, 1×10^5 HaCaT and

HeLa cancer cells were seeded in two different 96 well cell culture plates. After 24 h, the culture medium was replaced by a fresh medium containing various concentrations of complexes **C1–C3** and incubated further for 24 and 48 h respectively under a 5% CO_2 humidified atmosphere. The medium was then removed and 100 μL of fresh medium and 25 μL of 5 mg mL^{-1} MTT in phosphate buffered saline (PBS, pH 7.4) were added to each well for an additional 4 h. Finally, DMSO was added to dissolve the MTT formazan crystals. The absorbance of samples was measured at 570 nm with an TECAN plate reader. Cytotoxicity effect was revealed as the percentage of treated cells relative to untreated cells at 570 nm. Percent control was calculated using the following formula:

%Control= [Mean O. D. of drug treated well / mean O. D. of control well] ×100

4.6. DNA interaction studies

Electronic absorption spectroscopic studies were carried out using fixed concentration of compounds (SB, C1, C2 and C3) in DMSO solution (1%) with increasing concentration of Ct-DNA in 5 mM Tris HCl/50 mM NaCl buffer, pH 7.5, following an earlier procedure[19, 34]. The purity of the Ct-DNA was verified by electronic absorption studies following the ratio of absorbances at 260 and 280 nm, which was 1.8 and suggested that the DNA was sufficiently free of protein. The DNA concentration per nucleotide was determined by examining the molar extinction coefficient of 6600 M^{-1} cm^{-1} at 260 nm. The intrinsic binding constants 'K_b' were calculated from the spectroscopic data using the following equation:

$$[DNA]/(\varepsilon_a - \varepsilon_f) = [DNA]/(\varepsilon_b - \varepsilon_f) + 1/K_b(\varepsilon_b - \varepsilon_f) \quad \text{.....(1)}$$

where 'ε_f' and 'ε_b' are the extinction coefficients of the free and fully bound complex, while 'ε_a' is the extinction coefficient observed for the absorption band at a given DNA concentration

and K_b is the equilibrium binding constant. From the plot of [DNA]/($\varepsilon_a - \varepsilon_f$) versus [DNA], the ratio of the slope to the intercept gives K_b.

4.7. ROS generation assay

Metal-complexes intracellular ROS generation levels were measured by DCFH2-DA (2′,7′-dichlorodihydrofluorescin diacetate) (Sigma-Aldrich). Briefly, HeLa cells (1×10^5 cells per well) were treated with different concentrations of metal-complex based on the IC_{50} value for 24 h at 37 °C under a humidified atmosphere of 5% CO_2. Fluorescent measurement was performed as described previously[43, 68].

4.8. Fluorescence staining of HeLa cells

Cells were seeded in 96 well plates and kept for 24 h at 37 °C in a humidified atmosphere of 5% CO_2. After that, cells were treated with 15 μM concentration of different complexes (C1-C3) for 24 h. Subsequently, cells were washed with 1× PBS and stained with 4′,6-diamidino-2-phenylindole, (DAPI) (5 μg mL^{-1}) solution. Cells were then washed with PBS and images were taken using a fluorescent microscope (Evos FL, Life technologies) in blue and red channels[67].

4.9. DNA oxidation measurement

DNA oxidation measurement was essentially done using 8-Oxo detection ELISA kit (Cayman chemicals) according to manufacturer's protocol and as described previously[43]. In brief, genomic DNA was extracted after 24 h from HeLa cells treated with different concentrations of metal complexes (5,10,15 μM) as well as from control cells using standard phenol/chloroform method. To prevent accidental DNA oxidation during extraction procedure, cell lysis buffer was supplemented with 1 mM ascorbic acid and 1 mM deferoxamine (iron

chelator). Isolated DNA were digested using nuclease P1 (sigma) followed by alkaline phosphatase (NEB). Samples were prepared and used for ELISA kit.

Acknowledgements

M.A.M gratefully acknowledges Council of Scientific and Industrial Research (CSIR), New Delhi, India for the financial assistance in the form of Senior Research Fellowship for this work [File No.: 09/466(0215)2K19 EMR-1].

Author Contributions

MYW and AAH designed and supervised the project. MAM, MKR and AM performed experiments, analyzed data, prepared Figures and wrote the main manuscript text. All authors discussed the results and implications and commented on the manuscript at all stages.

Additional Information

Competing Interests: The authors declare no competing interests.

References

1. Rebecca L. Siegel, Kimberly D. Miller, Ahmedin Jemal, Cancer Statistics, 2020, *CA Cancer J. Clin.***70**, 7–30 (2020)
2. Fares, J., Fares, M.Y., Khachfe, H.H., Salhab H. A, & Fares Y., Molecular principles of metastasis: a hallmark of cancer revisited. *Sig Transduct Target Ther* **5,** 28 (2020).
3. Klein, C.A. Cancer progression and the invisible phase of metastatic colonization. *Nat Rev Cancer* **20,** 681–694 (2020).
4. Jin, X., Demere, Z., Nair, K., Ali, A., Ferraro, G. B., Natoli, T., ... & Golub, T. R. A metastasis map of human cancer cell lines. *Nature* **588**(7837), 331-336 (2020).

5. Karuna Ganesh & Joan Massagué Targeting metastatic cancer, *Nature Medicine* **27**, 34–44 (2021).
6. Stephen P. Jackson and Jiri Bartek, The DNA-damage response in human biology and disease, *Nature* **461**(7267): 1071–1078 (2009).
7. Rebecca A. Alderden, Matthew D. Hall, and Trevor W. Hambley, The Discovery and Development of Cisplatin, *Journal of Chemical Education* **83**, 728-734 (2006).
8. Fricker, S. P. Metal based drugs: from serendipity to design. *Dalton transactions* **43**, 4903-4917 (2007).
9. Barry, N. P., & Sadler, P. J. Exploration of the medical periodic table: towards new targets. *Chemical Communications* **49**(45), 5106-5131 (2013).
10. Baudino T.A. Targeted Cancer Therapy: The Next Generation of Cancer Treatment. *Curr Drug Discov Technol.* **12**(1),3-20 (2015).
11. Sawyers, C. Targeted cancer therapy. *Nature* **432,** 294–297 (2004).
12. Giovannetti E, Rodriguez J.A. Targeted therapies in cancer: where are we going? *Cancer Drug Resist* **1**, 82-86 (2018).
13. Ke, X., & Shen, L. Molecular targeted therapy of cancer: The progress and future prospect. *Frontiers in Laboratory Medicine* **1**(2), 69-75 (2017).
14. Talwar, V., Babu, K. P., & Raina, S. An overall review of targeted therapy in solid cancers. *Current Medicine Research and Practice* **7**(3), 99-105 (2017).
15. Ozaki T, Nakagawara A. Role of p53 in Cell Death and Human Cancers. *Cancers (Basel)* **3**(1), 994-1013 (2011).
16. Zilfou, J. T., & Lowe, S. W. Tumor suppressive functions of p53. *Cold Spring Harbor perspectives in biology* **1**(5), a001883 (2009).

17. Pandey, S., Pandey, L. K., Saxena, A. K., & Patel, N. The role of p53 gene in cervical carcinogenesis. *The Journal of Obstetrics and Gynecology of India* **66**(1), 383-388 (2016).

18. Chen J. The Cell-Cycle Arrest and Apoptotic Functions of p53 in Tumor Initiation and Progression. *Cold Spring Harb Perspect Med.* **6**(3), a026104 (2016).

19. Ashraf, R., Hamidullah., Hasanain, M., Praveen, P., Mayank, M., Singh, L. R., Siddiqui, M. Q., Rituraj, K., Koneni,V. S., & Jayanta, S. Coumarin-chalcone hybrid instigates DNA damage by minor groove binding and stabilizes p53 through post translational modifications. *Sci Rep* **7,** 45287 (2017).

20. Weller M. Predicting response to cancer chemotherapy: the role of p53. *Cell Tissue Res.* **292**(3), 435-45 (1998).

21. Hientz K., Mohr A., Bhakta-Guha D., Efferth T. The role of p53 in cancer drug resistance and targeted chemotherapy. *Oncotarget.* **8,** 8921-8946 (2017).

22. Martinez-Rivera M, Siddik Z.H. Resistance and gain-of-resistance phenotypes in cancers harboring wild-type p53. *Biochem Pharmacol* **83,** 1049–62 (2012).

23. Arnold, J. L. Targeting Therapies for the p53 Protein in Cancer Treatments, *Annual Review of Cancer Biology* **3,** 21-34(2019).

24. Brown, C.J., Cheok, C.F., Verma, C.S., Lane, D.P. Reactivation of p53: from peptides to small molecules. *Trends Pharmacol Sci.* **32**(1), 53-62 (2011).

25. Amarasena, I.U., Chatterjee, S., Walters, J.A., Wood-Baker, R., Fong, K.M. Platinum versus non-platinum chemotherapy regimens for small cell lung cancer. *Cochrane Database Syst Rev.* **8,** CD006849 (2015).

26. Malik, M. A., Dar, O. A., Gull, P., Wani, M. Y., & Hashmi, A. A. Heterocyclic Schiff base transition metal complexes in antimicrobial and anticancer chemotherapy. *MedChemComm* **9**(3), 409-436 (2018).

27. Bruijnincx, P. C., & Sadler, P. J. New trends for metal complexes with anticancer activity. *Current opinion in chemical biology* ***12***(2), 197-206 (2008).

28. Ndagi, U., Mhlongo, N., Soliman, M. E. Metal complexes in cancer therapy - an update from drug design perspective. *Drug Des Devel Ther.* **11,** 599-616(2017).

29. Jia, P., Ouyang, R., Cao, P., Tong, X., Zhou, X., Lei, T., ... & Zhou, S. Recent advances and future development of metal complexes as anticancer agents. *Journal of Coordination Chemistry* **70**(13), 2175-2201 (2017).

30. Zhang, Z., Wang, H., Yan, M., Wang, H., & Zhang, C. Novel copper complexes as potential proteasome inhibitors for cancer treatment. *Molecular medicine reports* **15**(1), 3-11 (2017).

31. Marzano C, Pellei M, Tisato F, Santini C. Copper complexes as anticancer agents. *Anticancer Agents Med Chem.* **9**(2), 185-211 (2009).

32. Santini, C., Pellei, M., Gandin, V., Porchia, M., Tisato, F., & Marzano, C. Advances in copper complexes as anticancer agents. *Chemical reviews* **114**(1), 815-862 (2014).

33. Graf, N., Lippard, S. J. Redox activation of metal-based prodrugs as a strategy for drug delivery. *Adv Drug Deliv Rev* **64,** 993-1004 (2012).

34. Malik, M. A., Raza, M. K., Dar, O. A., Abid, M., Wani, M. Y., Al-Bogami, A. S., & Hashmi, A. A. Probing the antibacterial and anticancer potential of tryptamine based mixed ligand Schiff base Ruthenium (III) complexes. *Bioorganic chemistry* **87**, 773-782 (2019).

35. Marloye, M., Berger, G., Gelbcke, M., & Dufrasne, F. A survey of the mechanisms of action of anticancer transition metal complexes. *Future medicinal chemistry* **8**(18), 2263-2286 (2016).

36. Alessio, E., & Guo, Z. Metal anticancer complexes–activity, mechanism of action, future perspectives. *Eur. J. Inorg. Chem*. **12**, 1539-1540 (2017)

37. Nair, M. S., & Joseyphus, R. S. Synthesis and characterization of Co (II), Ni (II), Cu (II) and Zn (II) complexes of tridentate Schiff base derived from vanillin and DL-α-aminobutyric acid. *Spectrochimica Acta Part A: Molecular and Biomolecular Spectroscopy* **70**(4), 749-753 (2008).

38. Lever, A. B. P. Inorganic electronic spectroscopy. 2nd Edition, Elsevier, Amsterdam (1984).

39. Gałczyńska, K., Drulis-Kawa, Z., & Arabski, M. Antitumor Activity of Pt (II), Ru (III) and Cu (II) Complexes. *Molecules* **25**(15), 3492 (2020).

40. Tan, C. P., Lu, Y. Y., Ji, L. N., & Mao, Z. W. Metallomics insights into the programmed cell death induced by metal-based anticancer compounds. *Metallomics* **6**(5), 978-995 (2014).

41. Arbyn, M., Weiderpass, E., Bruni, L., de Sanjosé, S., Saraiya, M., Ferlay, J., & Bray, F. Estimates of incidence and mortality of cervical cancer in 2018: a worldwide analysis. *The Lancet Global Health* **8**(2), e191-e203 (2020).

42. Salem, O. M., Vilková, M., Janočková, J., Jendželovský, R., Fedoročko, P., Imrich, J., & Kožurková, M. Synthesis, spectral characterization, DNA binding ability and anti-cancer screening of new acridine-based derivatives. *Medicinal Chemistry Research* **26**(10), 2309-2321 (2017).

43. Salehi, F., Behboudi, H., Kavoosi, G., & Ardestani, S. K. Oxidative DNA damage induced by ROS-modulating agents with the ability to target DNA: A comparison of the biological characteristics of citrus pectin and apple pectin. *Scientific reports* **8**(1), 1-16 (2018).

44. Bhat, S. S., Kumbhar, A. A., Heptullah, H., Khan, A. A., Gobre, V. V., Gejji, S. P., & Puranik, V. G. Synthesis, electronic structure, DNA and protein binding, DNA

cleavage, and anticancer activity of fluorophore-labeled copper (II) complexes. *Inorganic chemistry* **50**(2), 545-558 (2011).

45. Pages, B. J., Ang, D. L., Wright, E. P., & Aldrich-Wright, J. R. Metal complex interactions with DNA. *Dalton transactions* **44**(8), 3505-3526 (2015).
46. Kate, A. N., Kumbhar, A. A., Khan, A. A., Joshi, P. V., & Puranik, V. G. Monitoring cellular uptake and cytotoxicity of copper (II) complex using a fluorescent anthracene thiosemicarbazone ligand. *Bioconjugate chemistry* **25**(1), 102-114 (2014).
47. Zhang, J., Xu, M., DNA fragmentation in apoptosis. *Cell Res* **10**, 205–211 (2000).
48. Deavall, D. G., Martin, E. A., Horner, J. M. & Roberts, R. Drug-induced oxidative stress and toxicity. *Journal of toxicology* **2012**, (2012).
49. Mangal, D., Vudathala, D., Park, J. H., Lee, S. H., Penning, T. M., & Blair, I. A. Analysis of 7, 8-dihydro-8-oxo-2′-deoxyguanosine in cellular DNA during oxidative stress. *Chemical research in toxicology* **22**(5), 788-797 (2009).
50. Porter, A. G. Jaenicke RU. Emerging roles of caspase-3 in apoptosis. *Cell Death Differ* **6**, 99-104 (1999).
51. McComb, S., Chan, P. K., Guinot, A., Hartmannsdottir, H., Jenni, S., Dobay, M. P., ... & Bornhauser, B. C. Efficient apoptosis requires feedback amplification of upstream apoptotic signals by effector caspase-3 or-7. *Science advances* **5**(7), eaau9433 (2019).
52. Drew, H. R., Wing, R. M., Takano, T., Broka, C., Tanaka, S., Itakura, K., and Dickerson, R. E. Structure of a B-DNA dodecamer: conformation and dynamics. PNAS, **78 (4)**, 2179-2183 (1981)
53. Trott, O., & Olson, A. J. AutoDock Vina: improving the speed and accuracy of docking with a new scoring function, efficient optimization, and multithreading. *Journal of computational chemistry* **31**(2), 455-461 (2010).

54. Cho, Y., Gorina, S., Jeffrey, P.D., & Pavletich, N.P. Crystal structure of a p53 tumor suppressor-DNA complex: understanding tumorigenic mutations. *Science*. **265**, 346-55 (1994).

55. Haas, K. L., & Franz, K. J. Application of metal coordination chemistry to explore and manipulate cell biology. *Chemical reviews* **109**(10), 4921-4960 (2009).

56. Sodhi, R. K., & Paul, S. Metal Complexes in Medicine: An Overview and Update from Drug Design Perspective. *Canc Therapy & Oncol Int J.* **14**(2) 555883 (2019).

57. Ahn, G. O., Botting, K. J., Patterson, A. V., Ware, D. C., Tercel, M., & Wilson, W. R. (2006). Radiolytic and cellular reduction of a novel hypoxia-activated cobalt (III) prodrug of a chloromethylbenzindoline DNA minor groove alkylator. *Biochemical pharmacology* **71**(12), 1683-1694 (2006).

58. Parker, L. L., Lacy, S. M., Farrugia, L. J., Evans, C., Robins, D. J., O'Hare, C. C., ... & Stratford, I. J. A novel design strategy for stable metal complexes of nitrogen mustards as bioreductive prodrugs. *Journal of medicinal chemistry* **47**(23), 5683-5689 (2004).

59. Kamaraj, B., & Bogaerts, A. Structure and function of p53-DNA complexes with inactivation and rescue mutations: A molecular dynamics simulation study. PLoS ONE **10(8),** e0134638 (2015).

60. Garai A, Kumar A, Kastan, M., Bartek, J. Cell-cycle checkpoints and cancer. *Nature* **432**, 316–323 (2004).

61. Soengas, M.S., Alarcón, R.M., Yoshida, H., Giaccia, A.J., Hakem, R., Mak, T.W., & Lowe, S.W. Apaf-1 and caspase-9 in p53-dependent apoptosis and tumor inhibition. *Science* **284**, 156-9 (1999).

62. Fridman, J., & Lowe, S. Control of apoptosis by p53. *Oncogene* **22**, 9030–9040 (2003).

63. Ansari, K. I., Kasiri, S., Grant, J. D., & Mandal, S. S. Fe (III)-salen and salphen complexes induce caspase activation and apoptosis in human cells. *Journal of Biomolecular Screening* **16**(1), 26-35 (2011).

64. Kyzioł, A., Cierniak, A., Gubernator, J., Markowski, A., Jeżowska-Bojczuk, M., & Komarnicka, U. K. Copper (I) complexes with phosphine derived from sparfloxacin. Part III: multifaceted cell death and preliminary study of liposomal formulation of selected copper (I) complexes. *Dalton Transactions* **47**(6), 1981-1992 (2018).

65. Pradhan, N., Pratheek, B. M., Garai, A., Kumar, A., Meena, V. S., Ghosh, S., ... & Maiti, P. K. Induction of apoptosis by Fe (salen) Cl through caspase-dependent pathway specifically in tumor cells. *Cell biology international* **38**(10), 1118-1131 (2014).

66. Raman, N., Muthuraj, V., Ravichandran, S., & Kulandaisamy, A. Synthesis, characterisation and electrochemical behaviour of Cu (II), Co (II), Ni (II) and Zn (II) complexes derived from acetylacetone and p-anisidine and their antimicrobial activity. *Journal of Chemical sciences* **115**(3), 161-167 (2003).

67. Mohammed, A., Bhusainahalli, M. V., Ramesh, C., Yogesh, B. O., Kempegowda, M., Gopinath, S. K., Tapas, K. K. Nitric Oxide-Mediated Histone Hyperacetylation in Oral Cancer: Target for a Water-Soluble HAT Inhibitor, CTK7A. *Chem. & Biol.* **17**, 903-913 (2010).

68. Wu, D., Yotnda P. Production and detection of reactive oxygen species (ROS) in cancers. *J Vis Exp*. **57,** 3357 (2011).

Figures

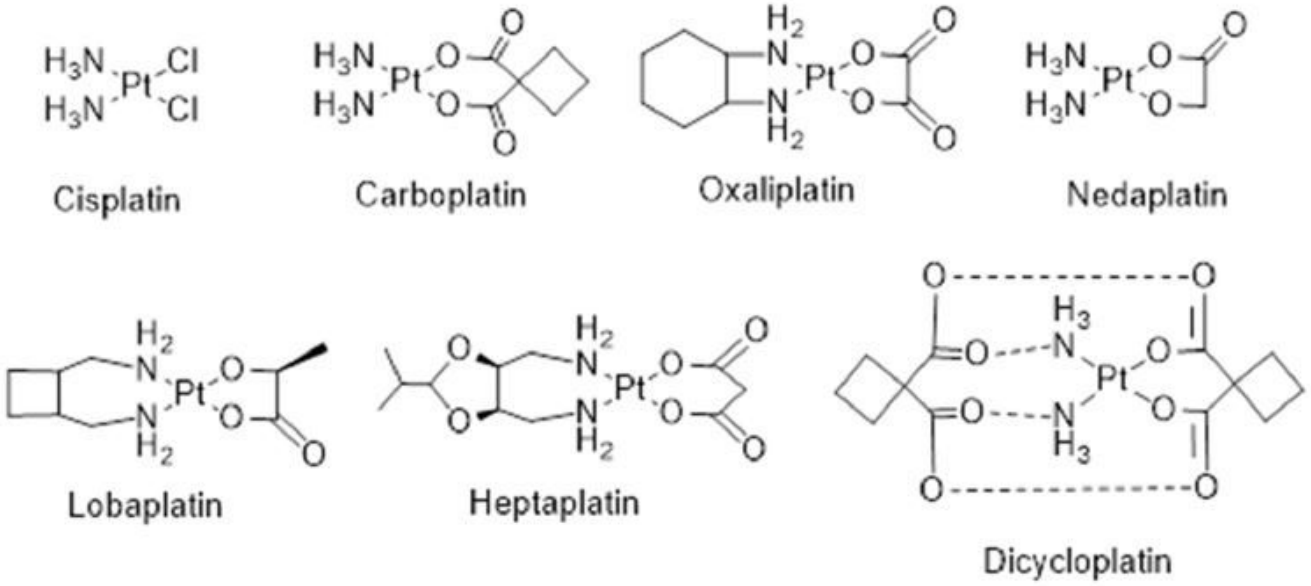

Figure 1

Molecular structures of some platinum anticancer drugs that are approved or undergoing clinical trials.

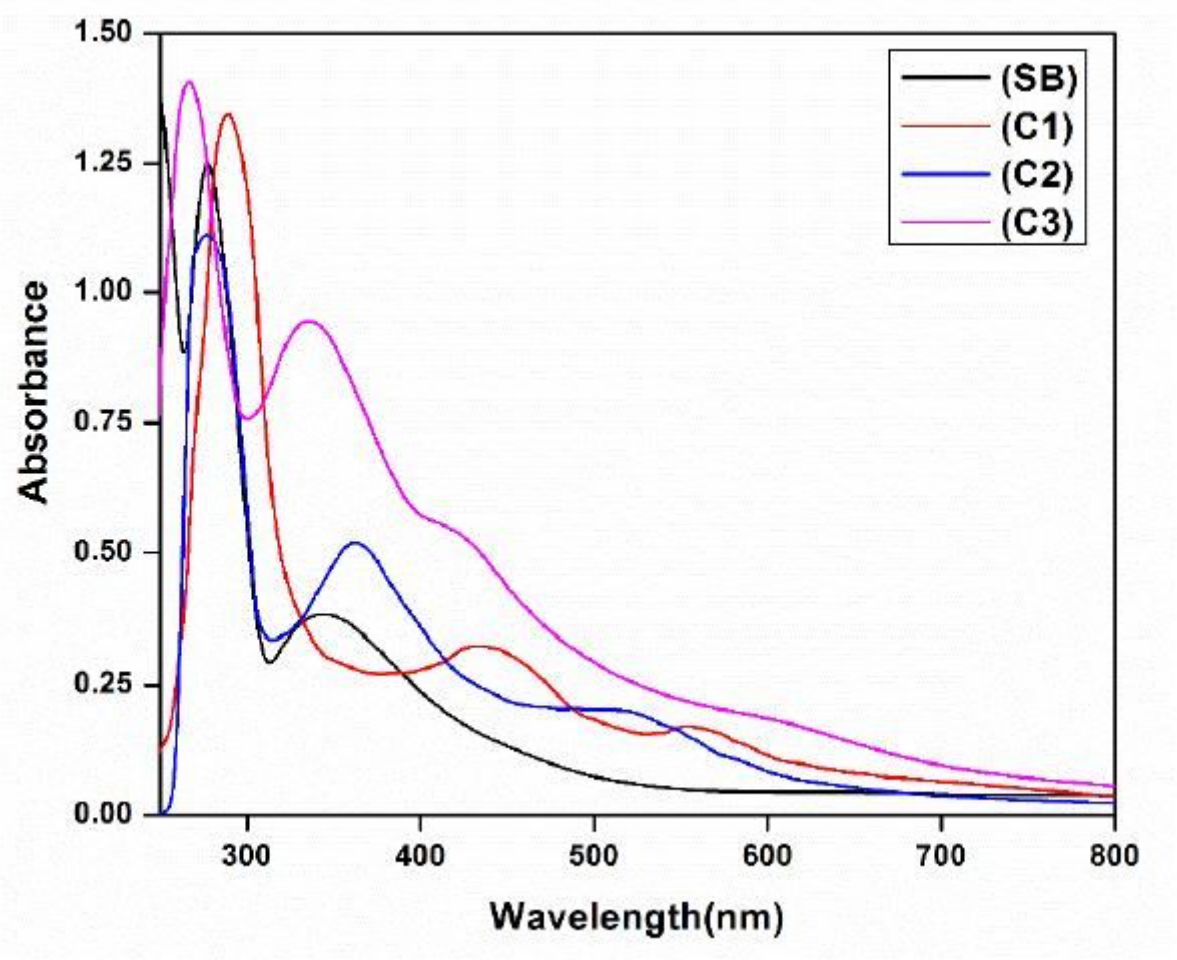

Figure 2

Electronic spectra of the ligand (SB) and metal complexes C1-C3.

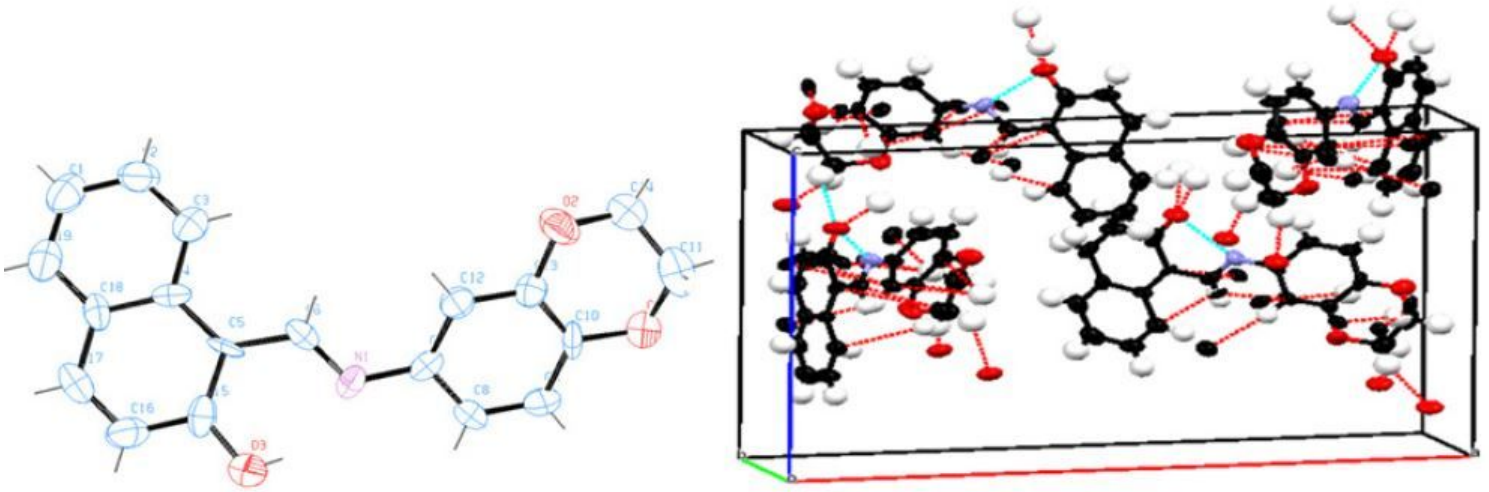

(A)

(B)

Figure 3

(A) ORTEP diagram of the ligand SB with thermal ellipsoids drawn at the 50% probability level. All hydrogen atoms are shown with single bonds radiating from the atoms for the sake of clarity. (B) Unit cell packing diagram of the ligand SB with hydrogen atoms showing hydrogen bonding and short contacts.

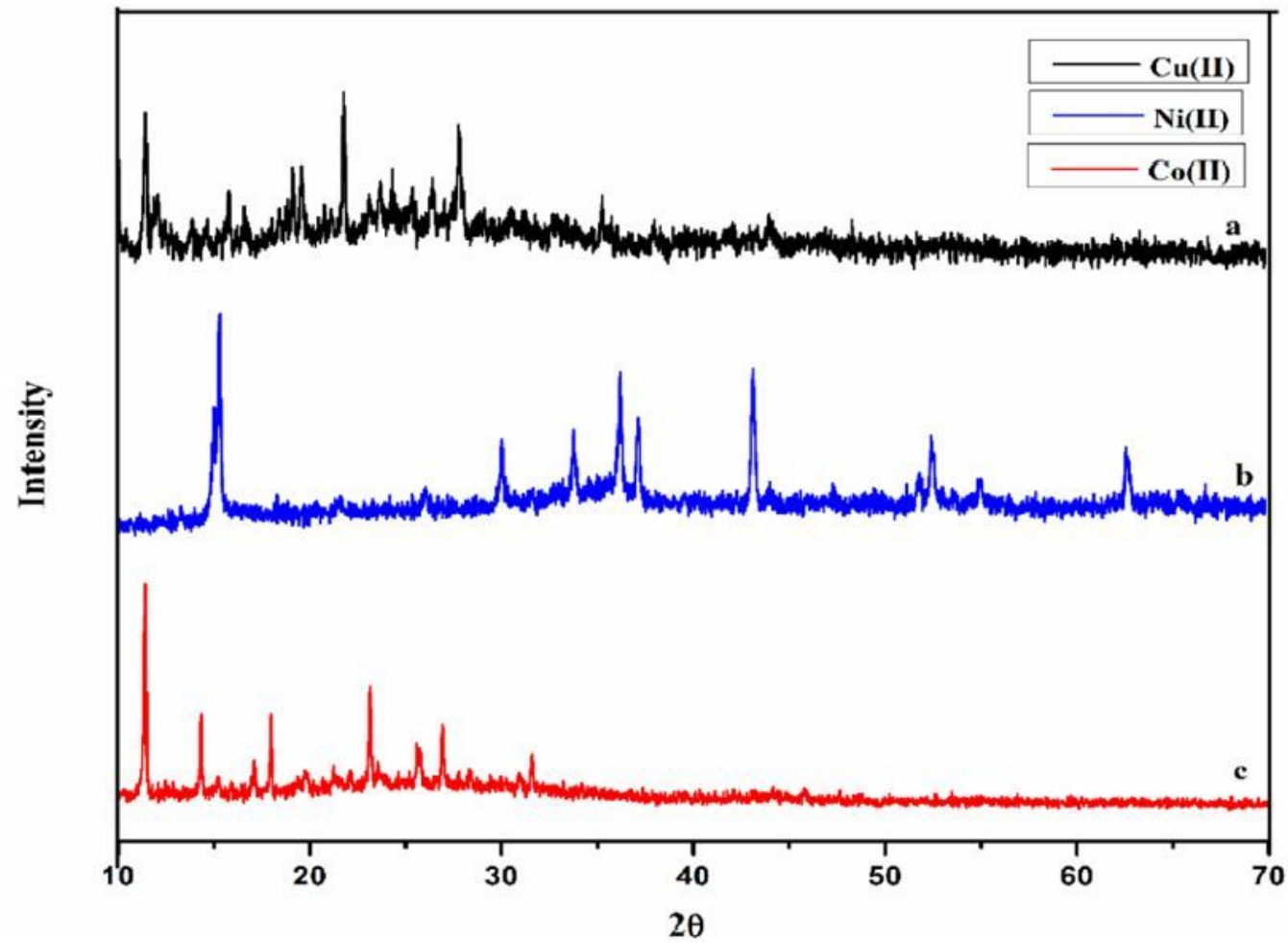

Figure 4

Powder X-ray diffraction pattern of (a) C1, (b) C2 and (c) C3 complex

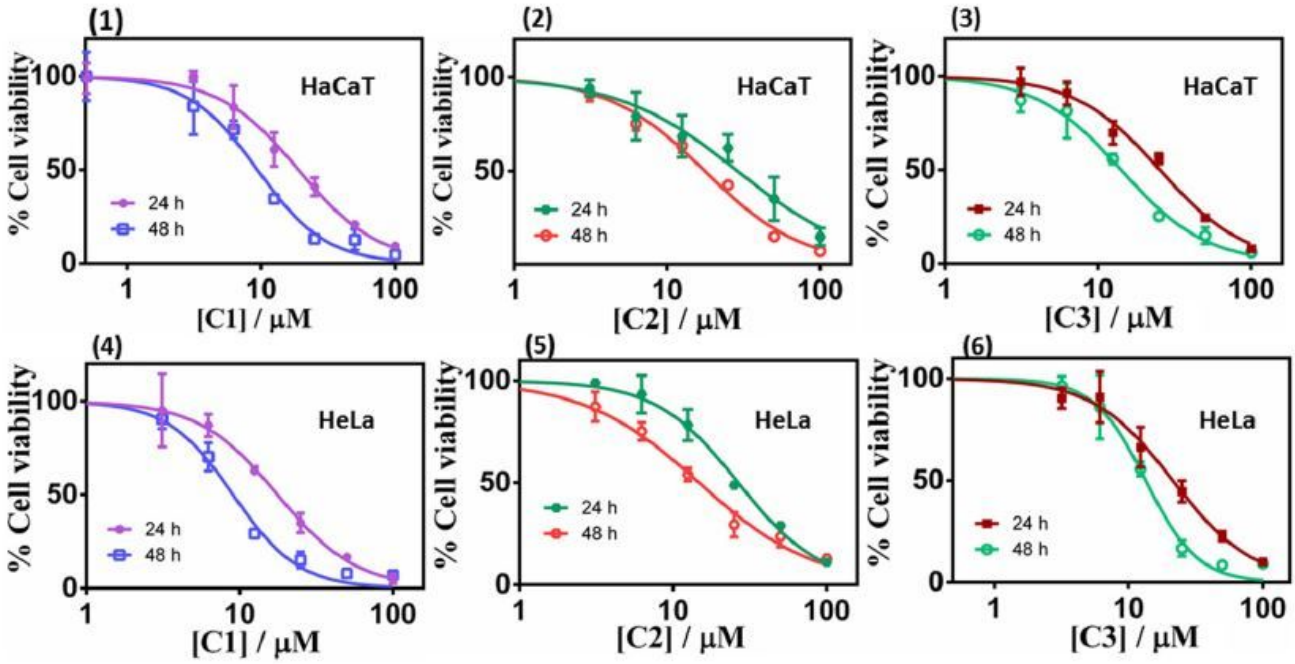

Figure 5

Cell viability plots (1)-(3) and (4)-(6) showing cytotoxicity of the respective complex C1–C3 in HaCaT and HeLa cells incubated for 24 h and 48 h respectively.

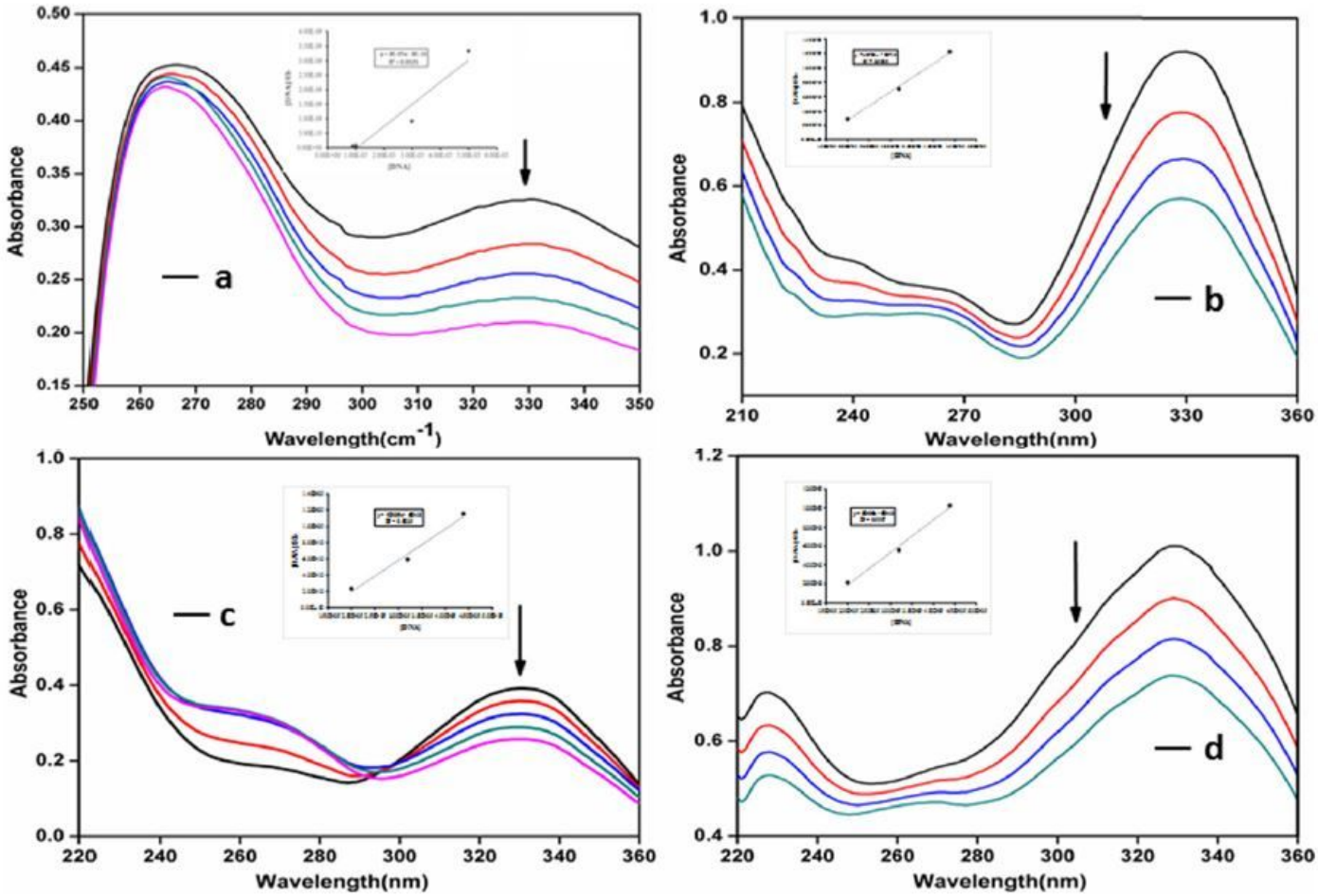

Figure 6

Absorption spectra of the ligand SB (a) and complexes C1 (b), C2 (c) and C3 (d) in the presence of increasing amounts of Ct-DNA at room temperature in 5 mM Tris-HCl/NaCl buffer (pH = 7.4) at 25°C. The arrow shows the absorbance changing upon increasing the DNA concentration. The plots of [DNA]/εa – εf) versus [DNA] for the ligand and the complexes are shown as insets in respective graphs (a), (b), (c) and (d).

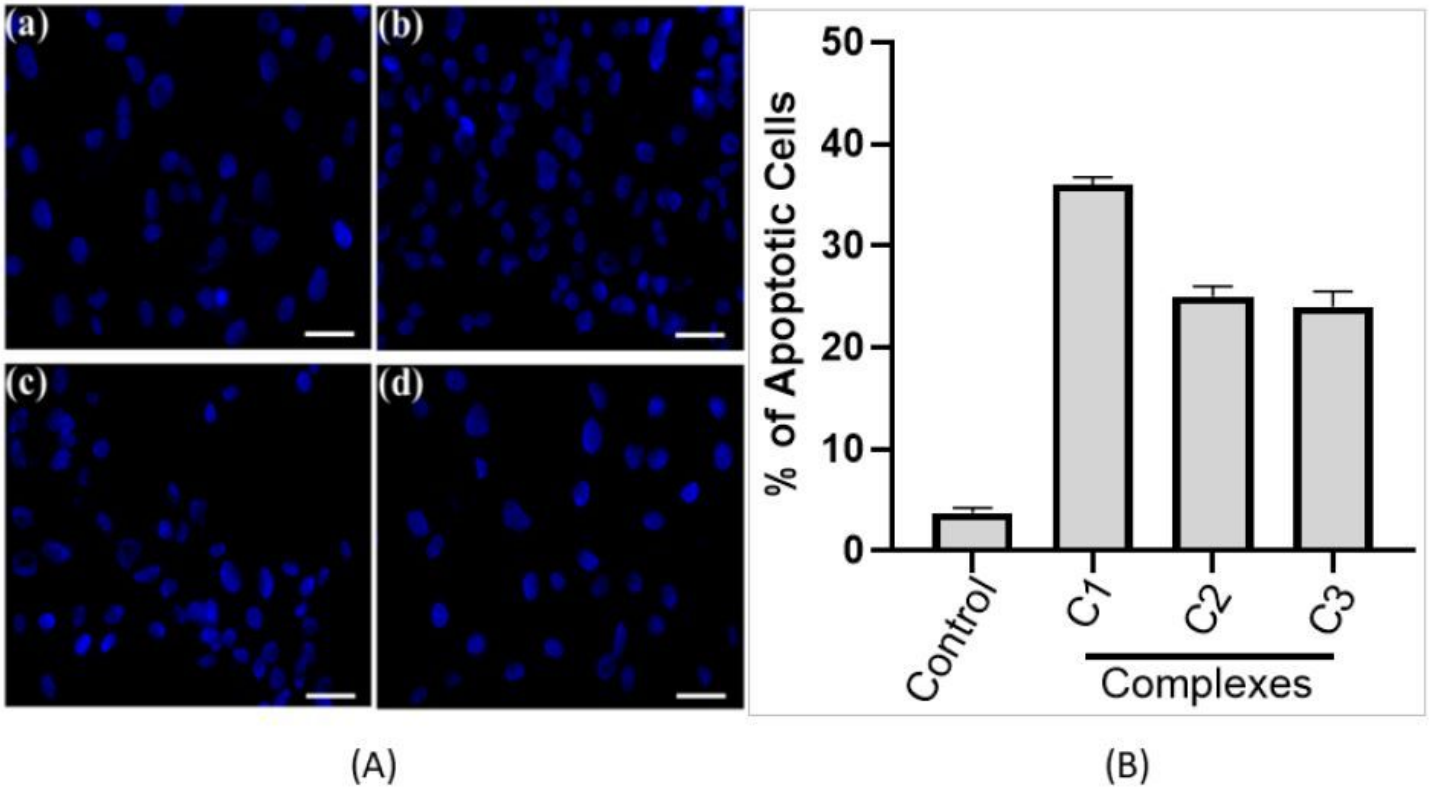

Figure 7

(A) Metal complexes induce cancer cell apoptosis. Florescence images of cervical cancer (HeLa) cells displaying morphological changes; (a) in absence of complexes (control) and on exposure to complexes (b) C1 complex, (c) C2 complex and (d) C3 complex detected with DAPI (blue) staining. Arrows indicate apoptotic nuclear fragmentation. Experiment was performed three times. (B) Representative figure is shown. Scale bars, 10 μm. (e) Bar graph represents the percentage of apoptotic cells determine by DAPI staining. Value represents the mean ± SD, n = 3.

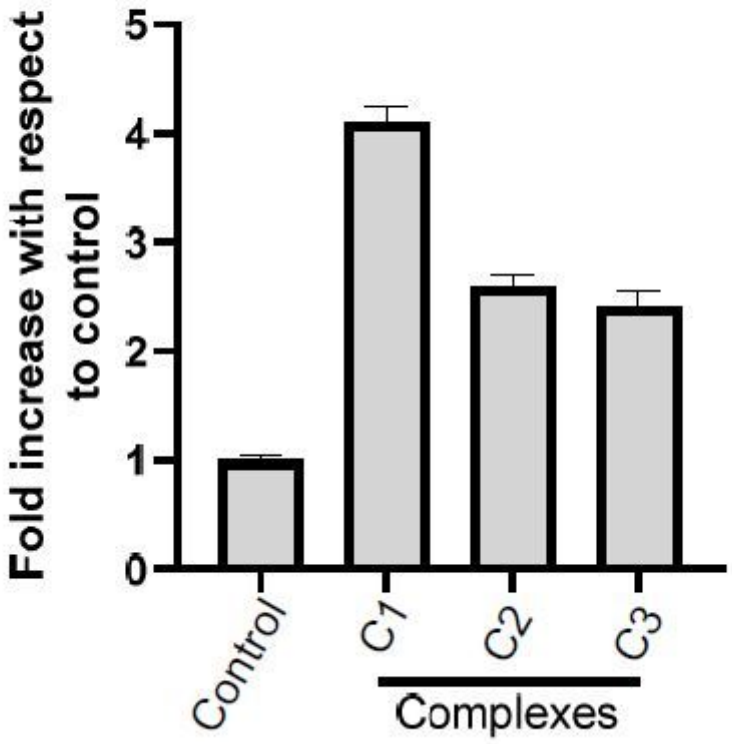

Figure 8

Determination of intracellular ROS level (DCF-DA assay) in human cervical cancer cell line HeLa, treated with solvent control and with different complex C1, C2 & C3 at 15μM; each for 24h. Results are expressed as fold increase with respect to control. Each value represent mean ± SD, of five independent experiments.

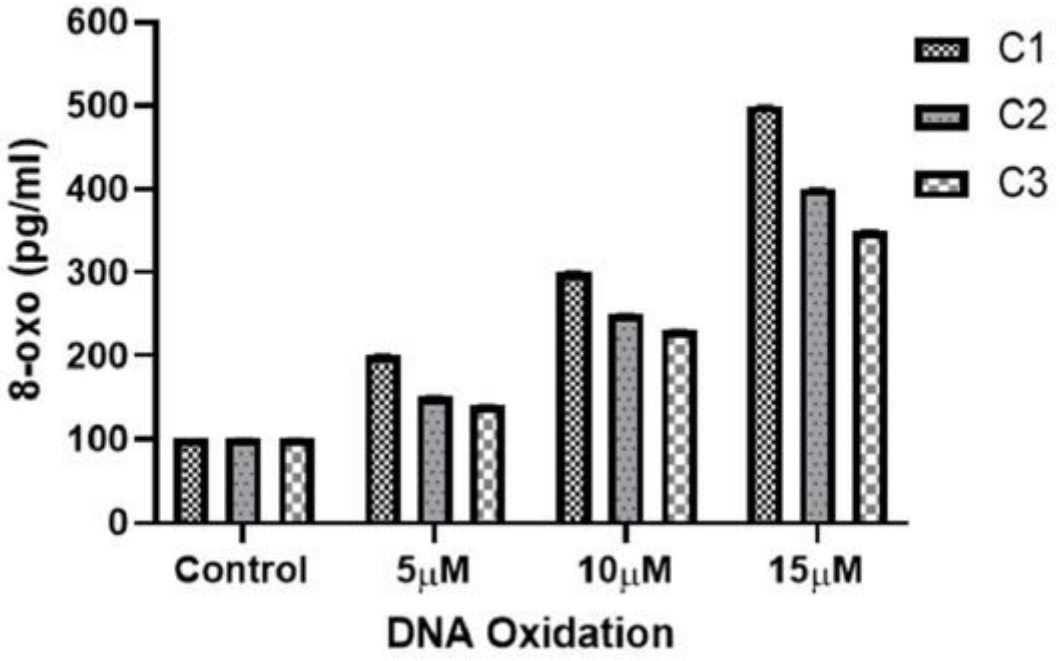

Figure 9

Determination of 8-oxo-dG of HeLa cells genomic DNA. HeLa cells were incubated with increasing concentrations of metal-complexes for 24 h and the amount of 8-oxo-dG formation was assessed using ELISA kit (see methods). Each value represent mean ± SD, of three independent experiments.

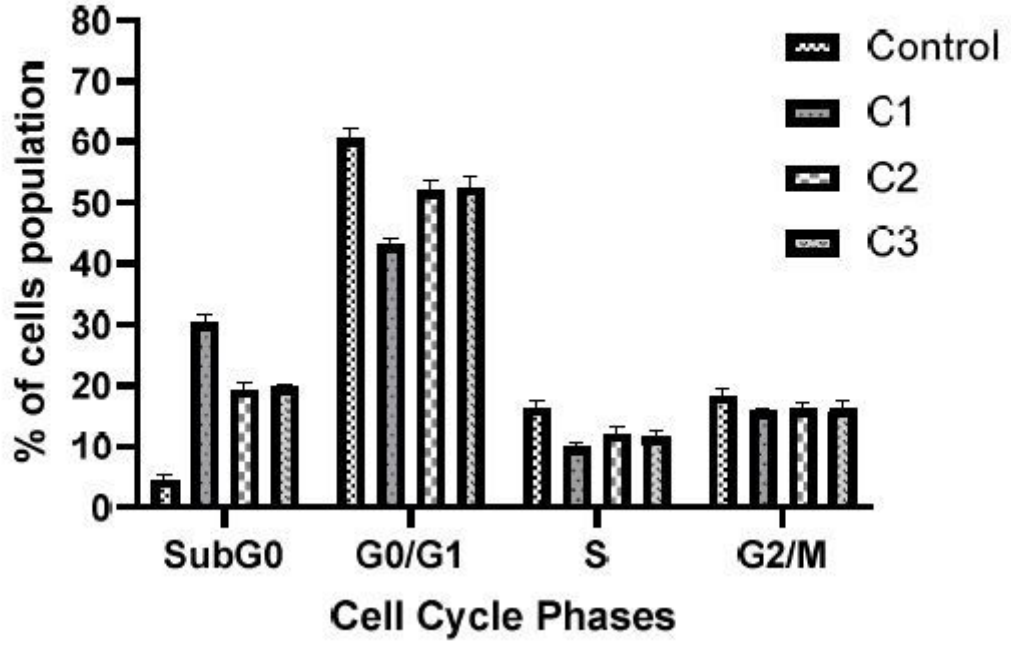

Figure 10

Metal complexes induce apoptosis in HeLa cancer cells. Cell cycle analysis was performed upon treatment of cells with 15 μM of metal complexes for 24 hours. After fixation, cell cycle analysis was performed with propidium iodide staining. Bar graph represents the percentage of cell population in different phases of cell cycle. Value represents the mean ± SD from three independent experiments.

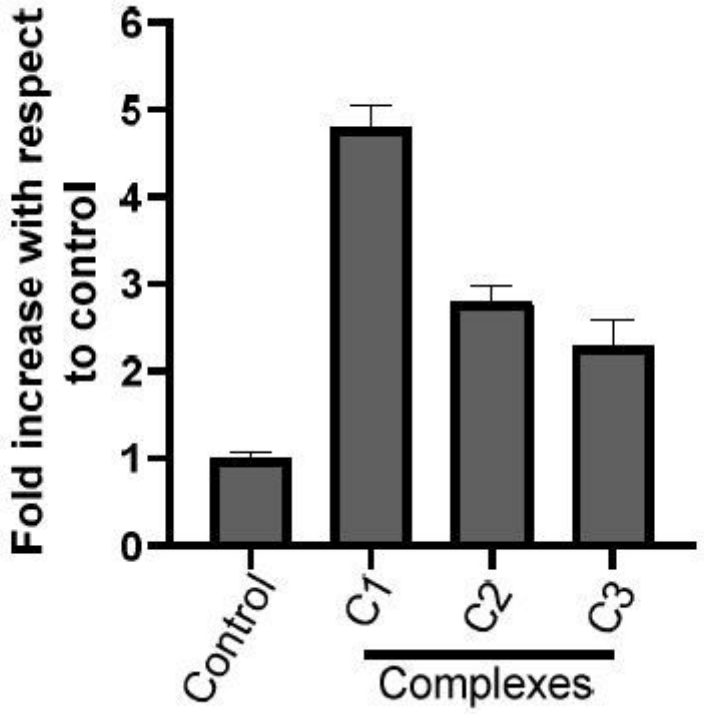

Figure 11

Effect of metal complexes on caspase-3 activity in HeLa cells. Cells were treated with solvent control and with different complex C1, C2 & C3 at 15μM; each for 24h and cytosolic extracts were used for caspase-3 activity. Results are expressed as fold increase with respect to control. Each value represent mean ± SD, of three independent experiments performed in duplicate.

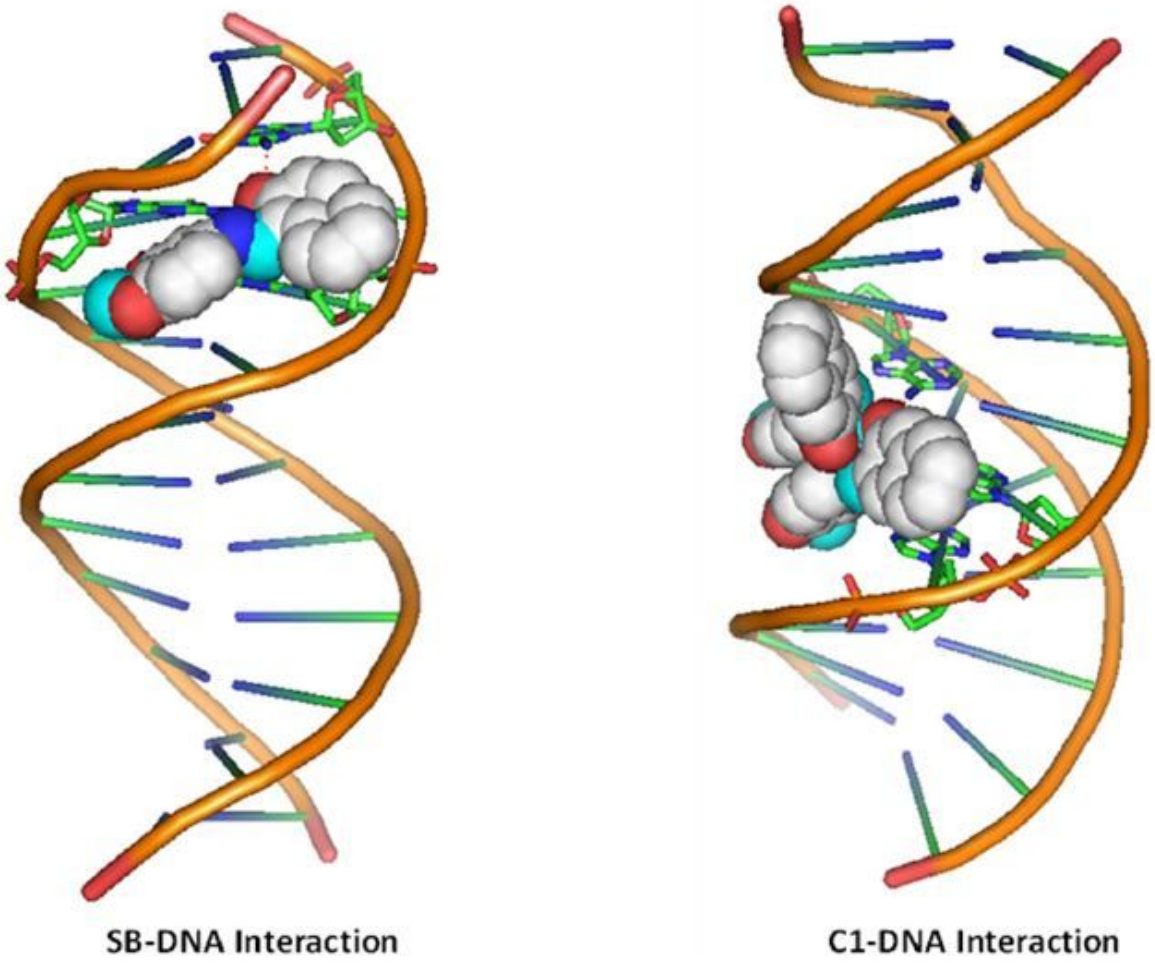

Figure 12

Docking study of the binding of SB and C1 to DNA.

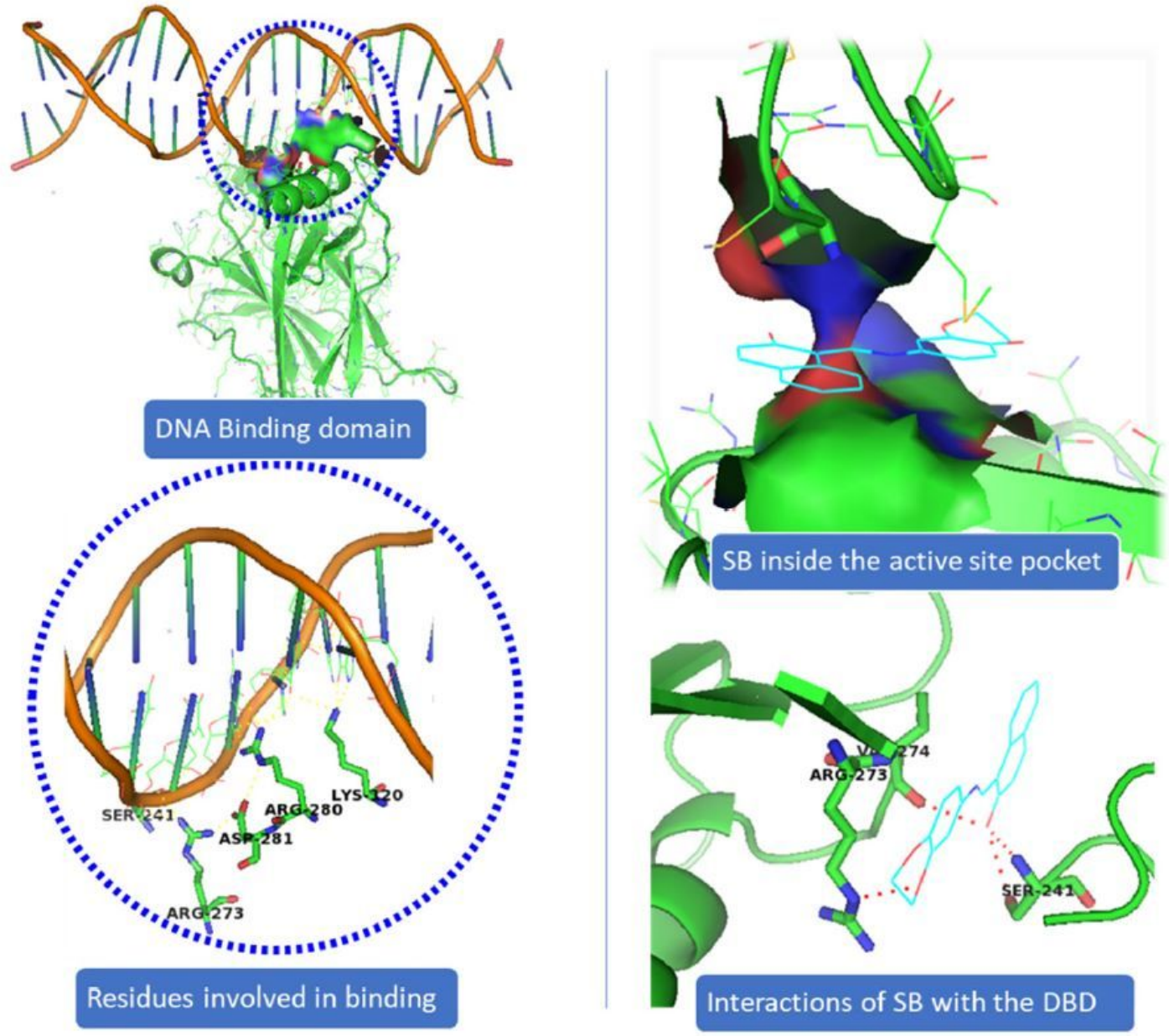

Figure 13

Docking study of the binding of SB to the p53DBD. P53 DBD shows interaction via LYS120, SER241, ARG273, ARG280, and ARG281 whereas, SB shows interaction with SER241, ARG273 and VAL274 inside the same binding pocket.

Supplementary Files

This is a list of supplementary files associated with this preprint. Click to download.

- SupportingInformation.docx